Electronic Supplementary Information for

Enhancing the Enantioselective Recognition and Sensing of Chiral Anions by Halogen Bonding

Jason Y. C. Lim,[a] Igor Marques,[b,c] Liliana Ferreira,[c] Vitor Félix,[b,c] and Paul D. Beer*[a]

[a] Chemistry Research Laboratory, Department of Chemistry, University of Oxford, Mansfield Road, Oxford, OX1 3TA, UK.
[b] Department of Chemistry, CICECO – Aveiro Institute of Materials, University of Aveiro, 3810-193 Aveiro, Portugal.
[c] Department of Medical Sciences, iBiMED – Institute of Biomedicine, University of Aveiro, 3810-193 Aveiro, Portugal.

E-mail: paul.beer@chem.ox.ac.uk

Contents

S1. Experimental

S1.1 General Information

All commercially available chemicals and solvents were used as received without further purification. All dry solvents were thoroughly degassed with N_2, dried through a Mbraun MPSP-800 column and used immediately. Water used was deionised and passed through a Milli-Q® Millipore machine for microfiltration. TBTA (tris(benzyltriazolemethyl)amine) was prepared according to reported procedures.[1] Amberlite® was prepared by washing the commercial resin beads sequentially with 10 % NaOH (aq), water, 0.1 M NH_4PF_6 (aq), further water, and finally loaded with 0.1 M NH_4PF_6 (aq) before any anion exchange to the PF_6^- salt occurred.

NMR spectra were recorded on Bruker AVIII HD Nanobay 400 MHz, Bruker AVIII 500 MHz and Bruker AVIII 500 MHz (with ^{13}C cryoprobe) spectrometers. Low resolution electrospray ionisation mass spectrometry (ESI-MS) was performed using the Waters Micromass LCT for characterisation of compounds previously reported in the literature, and high resolution ESI-MS was recorded using Bruker microTOF spectrometer for novel compounds.

S1.2 Synthetic Procedures

S1.2.1 Synthesis of (S)-BINOL receptors

Methoxy-protected *(S)*-BINOL **3** was prepared according to a literature procedure.[2]

Dialdehyde **4**

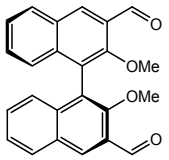

To a suspension of **3** (1.3 g, 4.14 mmol) in dry diethyl ether (40 mL) was added tetramethyl-ethylenediamine (TMEDA) (1.55 mL, 10.4 mmol) portionwise under N_2 at room temperature. After cooling the reaction to 0 °C, a 2.5 M solution of *n*-butyllithium in hexanes (7.3 mL, 18.3 mmol) was added dropwise, and the reaction was stirred at 0 °C for 1 hour before warming up to ambient temperature, then heated at reflux overnight. The resulting yellow-brown suspension was cooled to 0 °C, and anhydrous *N,N*-dimethylformamide (2.6 mL, 33.1 mmol) was added dropwise. Following which, the white suspension was warmed back up to room temperature and allowed to react for 2 hours, before 10 % HCl (aq.) (20 mL) was added to the reaction and stirred for 30 minutes. The aqueous and organic phases were separated, and the organic layer was washed successively with 1 M HCl (20 mL), saturated aqueous sodium bicarbonate (20 mL) and brine (20 mL), before finally drying with anhydrous $MgSO_4$. The solvent was removed to give a sticky yellow solid, which was purified by silica gel chromatography (EtOAc/ hexane 3:7) to furnish the product as a pale yellow solid (1.36 g, 89 %). **^{1}H-NMR** (400 MHz, $CDCl_3$) δ 10.61 (2H, s, C*H*O), 8.64 (2H, s, Ar*H*), 8.09 (2H, d, ^3J = 8.0 Hz, Ar*H*), 7.51 (2H, t, ^3J = 6.8 Hz, Ar*H*), 7.42 (2H, t, ^3J = 6.8 Hz, Ar*H*), 7.21 (2H, d, ^3J = 8.0 Hz, Ar*H*), 3.52 (6H, s, OCH_3); **^{13}C-NMR** (100 MHz, $CDCl_3$) δ 190.4, 156.7, 137.0, 132.3, 130.5, 130.0, 129.6, 128.7, 126.1, 125.6, 124.9, 63.2; **MS (ESI)** *m/z* calc. for $[M+H]^+$ = 371.1, found 371.1.

Bis-alcohol **5**

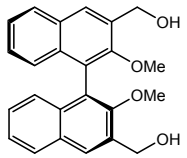

Dialdehyde **4** (1.25 g, 3.38 mmol) was dissolved in a 1:1 mixture of diethyl ether and ethanol (50 mL) with a minimum quantity of chloroform, and the reaction was chilled to 0 °C. Sodium borohydride (192 mg, 5.07 mmol) was added portionwise to the reaction and the reaction was stirred at 0 °C for 15 minutes before being warmed up to room temperature and reacted for 2 hours. Subsequently, the reaction was quenched with dropwise addition of 1 M HCl (CAUTION: brisk H_2 evolution!) till no further effervescence was observed. After the resulting biphasic mixture was stirred for 15 more minutes, the aqueous and organic layers were separated and the aqueous layer was extracted with ethyl acetate (4 x 20 mL). The combined organics were washed with saturated aqueous sodium bicarbonate and brine. Solvent removal *in vacuo* afforded the product as a sticky yellow solid in good purity (1.25 g, 99 %), which was used directly in the next step without further purification. **^{1}H-NMR** (400 MHz, $CDCl_3$) δ 8.02 (2H, s, Ar*H*), 7.91 (2H, d, ^3J = 8.0 Hz, Ar*H*), 7.42 (2H, t, ^3J = 8.0 Hz, Ar*H*), 7.26 (2H, t, ^3J = 7.2 Hz, Ar*H*), 7.18 (2H, d, ^3J = 7.2 Hz, Ar*H*), 5.05 (2H, d, ^3J = 12.0 Hz, CH_2OH), 4.93 (2H, d, ^3J = 12.0 Hz, CH_2OH), 3.33 (6H, s, OCH_3).

Bis-azide **6**

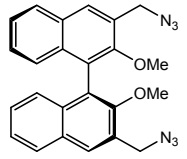

Bis-alcohol **5** (1.2 g, 3.2 mmol) was dissolved in toluene/ ethyl acetate/ dichloromethane 45: 45: 10 (40 mL) and chilled to 0 °C. Triethylamine (1.78 mL, 12.8 mmol) was added dropwise with stirring, followed by methanesulfonyl chloride (0.62 mL, 8.01 mmol). After the reaction proceeded overnight at room temperature, the reaction was checked by thin layer chromatography to ensure completion, before 1 M HCl (30 mL) was added to the reaction and stirring for a further 15 minutes. The aqueous and organic layers were then separated, and the aqueous layer was extracted with ethyl acetate (4 x 30 mL). The combined organics were dried with brine and anhydrous $MgSO_4$, before the solvent was removed to afford the bis-mesylate as a yellow viscous oil. Immediately, the product was taken up in DMSO (20 mL), and sodium azide (1.04 g, 16.0 mmol) was added slowly over 5 minutes, followed by 0.2 mL of water. After being left to stir overnight at room temperature under N_2, water (20 mL) and ethyl acetate (20 mL) were added to the reaction mixture and vigorously stirred till both organic and aqueous layers turned clear. Separation of both layers was then followed by extraction of the aqueous layer with ethyl acetate (4 x 20 mL). The combined organic layer was washed with brine (3 x 20 mL) and dried with $MgSO_4$. Following solvent removal, purification by silica gel chromatography (ethyl acetate/ hexane 1:3) afforded **6** as a sticky white solid (1.02 g, 75 %). **^{1}H-NMR** (400 MHz, $CDCl_3$) δ 8.00 (2H, s,

Ar*H*), 7.93 (2H, d, ^3J = 6.8 Hz, Ar*H*), 7.45 (2H, t, ^3J = 6.8 Hz, Ar*H*), 7.30 (2H, t, ^3J = 6.8 Hz, Ar*H*), 7.20 (2H, d, ^3J = 6.8 Hz, Ar*H*), 4.68 (4H, m, CH_2N$_3$), 3.31 (6H, s, OCH_3); **^{13}C-NMR** (100 MHz, $CDCl_3$) δ 154.7, 134.4, 130.3, 130.0, 128.9, 128.2, 127.0, 125.7, 125.3, 124.2, 61.0, 50.9; **MS (ESI)** *m/z* calc. for $[M+Na]^+$ = 447.2, found 447.2.

General Procedure for synthesis of XB (S)-BINOL iodotriazole receptor precursors

'One-pot' iodoclick procedure used was slightly modified from that reported by Zhu.[3]

Acetonitrile and THF were mixed in a 1:1 ratio and degassed by vigorous bubbling with N_2 for 10 minutes prior to the reaction. Sodium iodide (8.8 eqv.) was mixed with acetonitrile/ THF 1:1 (2 mL), and copper(II) perchlorate hexahydrate (4.4 eqv.) was added portionwise to the reaction, and the resulting dark brown mixture was stirred for 5 minutes under N_2. To this mixture was added TBTA (0.1 eqv.), 1,8-diazabicyclo-undec-7-ene (DBU) (2.2 eqv.), bis-azide **6** (1.0 eqv.) and the appropriate terminal alkyne (2.2 eqv.) successively. The reaction was stirred overnight in the dark under N_2, before it was diluted with chloroform (20 mL). The resulting suspension was washed with 10 % aqueous ammonia (2 x 10 mL), and the aqueous layer was back-extracted with chloroform (10 mL). The combined organics were then dried with brine and $MgSO_4$. Following solvent removal *in vacuo*, purification was achieved by silica gel chromatography.

General Procedure for synthesis of HB (S)-BINOL prototriazole receptor precursors

Bis-azide **6** (1.0 eqv.) was dissolved in dichloromethane (2 mL), and the appropriate terminal alkyne (2.1 eqv.) , TBTA (0.1 eqv.), tetrakis(acetonitrile)copper(I) hexafluorophosphate (0.3 eqv.) and diisopropylethylamine (3.0 eqv.) were added successively. The reaction was reacted for 16 h overnight before being diluted with chloroform (20 mL). The mixture was washed with 10 % aqueous ammonia (10 mL), followed by water (10 mL) and brine. After drying with $MgSO_4$, the solvent was removed and purification by silica gel chromatography afforded the products in good purity.

XB Receptor precursor **7.XB**

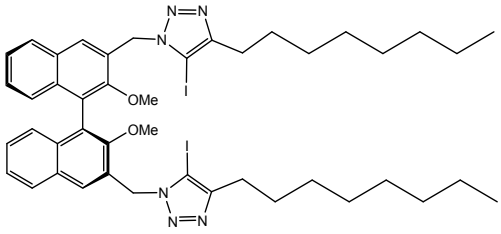

Quantities of reagents used: **6** (85 mg, 0.20 mmol), 1-decyne (79 µL, 0.44 mmol), sodium iodide (264 mg, 1.76 mmol), copper(II) perchlorate hexahydrate (326 mg, 0.88 mmol), DBU (66 µL, 0.44 mmol), TBTA (10 mg, 0.02 mmol). Silica gel chromatography (2 % MeOH in CH_2Cl_2 as eluent) furnished product **7.XB** was obtained as a viscous colourless oil (159 mg, 83 %). **^{1}H-NMR** (400 MHz, $CDCl_3$) δ 7.75 (2H, d, ^3J = 6.4 Hz, Ar*H*), 7.40 (2H, t, ^3J = 6.4 Hz, Ar*H*), 7.27 (4H, m, Ar*H*), 7.17 (2H, ^3J = 6.8 Hz, Ar*H*), 5.89 (4H, m, CH_2-triazoles), 3.30 (6H, s, OCH_3), 2.75 (4H, t, ^3J = 6.4 Hz, alkyl-*H*), 1.76 (4H, m, alkyl-*H*), 1.28-1.38 (20H, m, alkyl-*H*), 0.89 (6H, t, ^3J = 5.4 Hz, alkyl-*H*); **^{13}C-NMR** (100 MHz,

$CDCl_3$) δ 153.8, 134.1, 130.3, 128.3, 128.2, 127.1, 125.6, 125.3, 123.8, 77.2, 60.9, 31.9, 29.3, 29.2, 29.1, 28.9, 26.2, 22.7, 14.1 (missing peaks due to overlap); **MS** (ESI +ve) *m/z* 953.2465 ($[M+H]^+$, $C_{44}H_{55}O_2N_6I_2$, calc. 953.2471).

HB Receptor precursor **7.HB**

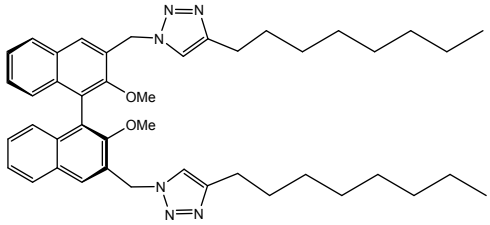

Quantities of reagents used: **6** (60 mg, 0.14 mmol), 1-decyne (53 µL, 0.30 mmol), tetrakis(acetonitrile)-copper(I) hexafluorophosphate (16 mg, 0.042 mmol), TBTA (7.5 mg, 0.014 mmol), diisopropylethylamine (74 µL, 0.42 mmol). Silica gel chromatography (3 % MeOH in CH_2Cl_2 as eluent) furnished the product **7.HB** was obtained as a colourless viscous oil (64 mg, 65 %). **^{1}H-NMR** (400 MHz, $CDCl_3$) δ 7.75 (2H, d, ^3J = 6.8 Hz, Ar*H*), 7.65 (2H, s, triazole-*H*), 7.33 (4H, m, Ar*H*), 7.20 (2H, t, ^3J = 6.8 Hz, Ar*H*), 7.07 (2H, d, ^3J = 6.8 Hz, Ar*H*), 5.64-5.77 (4H, m, CH_2-triazoles), 3.09 (6H, s, OCH_3), 2.66 (4H, t, ^3J = 6.4 Hz, alkyl-*H*), 1.59 (4H, m, alkyl-*H*), 1.17-1.28 (20H, m, alkyl-*H*), 0.78 (6H, t, ^3J = 6.4 Hz, alkyl-*H*); ; **^{13}C-NMR** (100 MHz, $CDCl_3$) δ 154.2, 148.8, 134.3, 130.3, 130.0, 128.4, 128.3, 127.3, 125.5, 125.5, 124.1, 121.1, 60.8, 49.9, 31.8, 29.5, 29.3, 29.2, 25.7, 22.6, 14.1; **MS** (ESI +ve) *m/z* 701.4530 ($[M+H]^+$, $C_{44}H_{57}O_2N_6$, calc. 701.4538).

Ferrocene-appended XB Receptor precursor **8.XB**

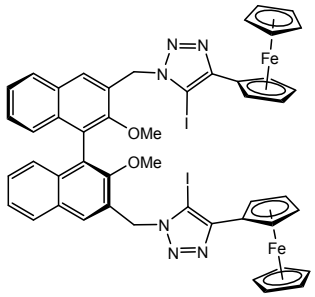

Quantities of reagents used: **6** (46 mg, 0.11 mmol), ethynylferrocene (50 mg, 0.24 mmol), sodium iodide (145 mg, 0.97 mmol), copper(II) perchlorate hexahydrate (179 mg, 0.48 mmol), DBU (36 µL, 0.24 mmol), TBTA (5.3 mg, 0.01 mmol). Silica gel chromatography (1 % MeOH in CH_2Cl_2 as eluent) furnished product **8.XB** was obtained as a sticky orange solid (113 mg, 95 %). **^{1}H-NMR** (400 MHz, d_6-acetone) δ 7.88 (2H, d, ^3J = 6.8 Hz, Ar*H*), 7.40-7.44 (4H, m, Ar*H*), 7.31 (4H, t, ^3J = 6.8 Hz, Ar*H*), 7.17 (2H, ^3J = 6.8 Hz, Ar*H*), 5.98 (4H, m, CH_2-triazoles), 5.10 (4H, m, Fc*H*), 4.38 (4H, m, Fc*H*), 4.14 (10H, s, Fc*H*), 3.46 (6H, s, OCH_3); **^{13}C-NMR** (100 MHz, d_6-acetone) δ 154.1, 149.5, 134.0, 130.4, 129.5, 128.1, 128.1, 126.9, 125.5, 125.3, 124.1, 76.4, 75.6, 69.3, 68.6, 66.8, 60.3, 49.8; **MS** (ESI +ve) *m/z* 1118.9692 ($[M+Na]^+$, $C_{48}H_{38}O_2N_6Fe_2I_2Na$, calc. 1118.9737).

Ferrocene-appended HB Receptor precursor **8.HB**

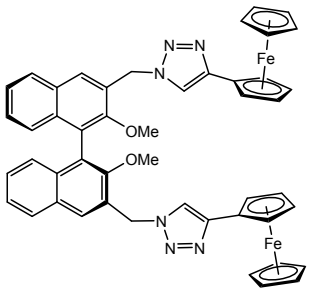

Quantities of reagents used: **6** (45 mg, 0.11 mmol), ethynylferrocene (47 mg, 0.22 mmol), tetrakis(acetonitrile)-copper(I) hexafluorophosphate (12 mg, 0.032 mmol), TBTA (5.6 mg, 0.011 mmol), diisopropylethylamine (55 µL, 0.32 mmol). Silica gel chromatography (2 % MeOH in CH_2Cl_2 as eluent) furnished the product **8.HB** was obtained as a sticky orange solid (71 mg, 79 %). **^{1}H-NMR** (400 MHz, d_6-DMSO) δ 8.24 (2H, s, triazole-*H*), 7.96 (2H, d, ^3J = 6.8 Hz, Ar*H*), 7.87 (2H, s, Ar*H*), 7.45 (4H, t, ^3J = 6.8 Hz, Ar*H*), 7.32 (2H, ^3J = 6.8 Hz, Ar*H*), 7.02 (2H, d, ^3J = 6.8 Hz, Ar*H*), 5.84 (4H, m, CH_2-triazoles), 4.75 (4H, m, Fc*H*), 4.30 (4H, m, Fc*H*), 4.01 (10H, s, Fc*H*), 3.20 (6H, s, OCH_3); **^{13}C-NMR** (100 MHz, d_6-DMSO) δ 154.5, 146.0, 134.1, 130.4, 130.3, 129.9, 128.7, 127.6, 125.9, 125.5, 124.4, 121.9, 76.4, 69.7, 68.8, 66.8, 60.8, 49.9 ; **MS** (ESI +ve) *m/z* 867.1770 ([M+Na]$^+$, $C_{48}H_{40}O_2N_6Fe_2Na$, calc. 867.1804)

General Procedure for Methylation of Receptor Precursors

The appropriate receptor precursor (1.0 eqv.) was dissolved in dry degassed acetonitrile (1.0 mL) and trimethyloxonium tetrafluoroborate (2.1 eqv.) was added portionwise. The reaction was left under N_2 for 2 days at room temperature in the dark. After checking that the reaction was complete by thin layer chromatography, methanol (0.1 mL) was added. The solvent was then removed *in vacuo* and following purification (see individual entries), anion exchange was performed using a hexafluorophosphate-loaded Amberlite ™ column using acetonitrile/ water 99-1 as eluent. Removal of solvent afforded the pure products as hexafluorophosphate salts.

XB Receptor **1.XB**

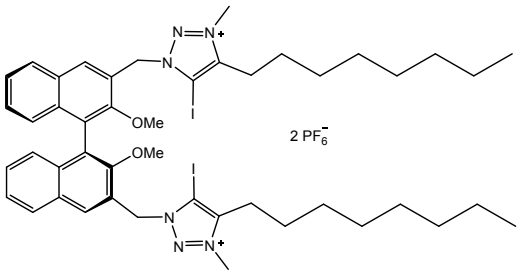

Quantities of reagents used: **7.XB** (25 mg, 0.026 mmol), trimethyloxonium tetrafluoroborate (8.2 mg, 0.055 mmol). Purification was achieved using preparatory thin layer chronmatography (5 % MeOH in CH_2Cl_2 as eluent). Following anion exchange, **1.XB** was obtained as a white solid (22 mg, 67 %). **^{1}H-NMR** (400 MHz, CD_3OD) δ 8.01 (2H, s, Ar*H*), 7.98 (2H, d, ^3J = 6.8 Hz, Ar*H*), 7.47 (2H, t, ^3J = 6.4 Hz, Ar*H*), 7.35 (2H, t, ^3J = 6.4 Hz, Ar*H*), 7.13 (2H, d, ^3J = 6.8 Hz, Ar*H*), 6.05 (4H, m, CH_2-

iodotriazolium), 4.32 (6H, s, iodotriazolium-CH_3), 3.27 (6H, s, OCH_3), 2.96 (4H, t, ^3J = 6.8 Hz, alkyl-*H*), 1.70 (4H, m, alkyl-*H*), 1.29-1.42 (20H, m, alkyl-*H*), 0.88 (6H, t, ^3J = 6.4 Hz, alkyl-*H*); **^{13}C-NMR** (100 MHz, CD_3OD) δ 153.9, 148.4, 134.7, 131.9, 130.2, 128.3, 127.5, 125.5, 125.2, 125.1, 123.4, 88.9, 60.0, 54.4, 37.4, 31.5, 28.8, 28.5, 28.4, 25.8, 23.6, 22.2, 13.0; **^{19}F-NMR** (376 MHz, CD_3OD) δ -74.6 (d, J = 708 Hz); **^{31}P-NMR** (162 MHz, CD_3OD) δ -141.6 (sept., J = 708 Hz); **MS** (ESI +ve) *m/z* 491.1423 ($[M]^{2+}$, $C_{46}H_{60}O_2N_6I_2$, calc. 491.1428).

HB Receptor **1.HB**

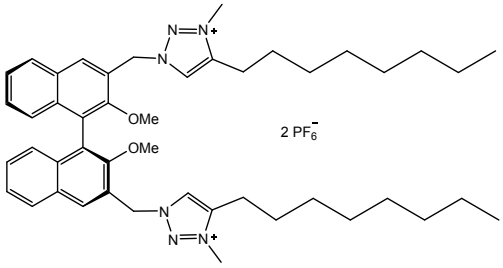

Quantities of reagents used: **7.HB** (20 mg, 0.029 mmol), trimethyloxonium tetrafluoroborate (9.3 mg, 0.063 mmol). Purification was achieved using preparatory thin layer chronmatography (5 % MeOH in CH_2Cl_2 as eluent). Following anion exchange, **1.HB** was obtained as a white solid (22 mg, 74 %). **^{1}H-NMR** (400 MHz, CD_3OD) δ 8.60 (2H, s, triazolium-*H*), 8.23 (2H, s, Ar*H*), 8.02 (2H, d, ^3J = 6.8 Hz, Ar*H*), 7.48 (2H, t, ^3J = 6.4 Hz, Ar*H*), 7.34 (2H, t, ^3J = 6.4 Hz, Ar*H*), 7.11 (2H, d, ^3J = 6.8 Hz, Ar*H*), 6.00 (4H, m, CH_2-iodotriazolium), 4.21 (6H, s, iodotriazolium-CH_3), 3.21 (6H, s, OCH_3), 2.86 (4H, t, ^3J = 6.8 Hz, alkyl-*H*), 1.74 (4H, m, alkyl-*H*), 1.28-1.40 (20H, m, alkyl-*H*), 0.87 (6H, t, ^3J = 6.4 Hz, alkyl-*H*); **^{13}C-NMR** (100 MHz, CD_3OD) δ 153.9, 148.4, 134.7, 131.9, 130.2, 128.3, 127.5, 125.5, 125.2, 125.1, 123.4, 88.9, 60.0, 54.4, 37.4, 31.5, 28.8, 28.5, 28.4, 25.8, 23.6, 22.2, 13.0; **^{19}F-NMR** (376 MHz, CD_3OD) δ -74.4 (d, J = 708 Hz); **^{31}P-NMR** (162 MHz, CD_3OD) δ -141.7 (sept., J = 708 Hz); **MS** (ESI +ve) *m/z* 365.2464 ($[M]^{2+}$, $C_{46}H_{62}O_2N_6$, calc. 365.2462).

Ferrocene-appended XB Receptor **2.XB**

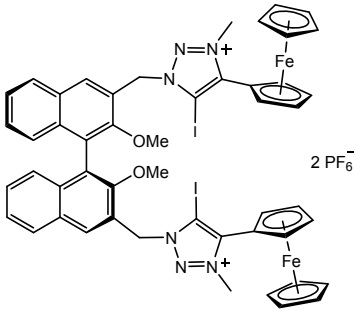

Quantities of reagents used: **8.XB** (30 mg, 0.027 mmol), trimethyloxonium tetrafluoroborate (8.4 mg, 0.057 mmol). Purification was achieved by column chromatography (2 % MeOH in CH_2Cl_2 as eluent) using activated Brockmann Grade 1 neutral alumina as the stationary phase. Following anion exchange, **2.XB** was obtained as an orange-brown solid (29 mg, 64 %). **^{1}H-NMR** (400 MHz, CD_3CN) δ 7.99 (2H, d, ^3J = 6.8 Hz, Ar*H*), 7.94 (2H, s, Ar*H*), 7.51 (2H, t, ^3J = 6.8 Hz, Ar*H*), 7.39 (2H, t, ^3J = 6.8 Hz, Ar*H*), 7.15 (2H, d, ^3J = 6.8 Hz, Ar*H*), 6.00 (4H, m, CH_2-iodotriazolium), 5.02 (4H, m, Fc*H*), 4.72 (4H, s, Fc*H*), 4.36 (6H, s, iodotriazolium-CH_3), 4.34 (10H, s, Fc*H*), 3.34 (6H, s, OCH_3); **^{13}C-NMR** (100 MHz,

CD_3CN) δ 154.6, 147.7, 135.1, 131.4, 130.7, 128.5, 128.4, 126.5, 126.0, 125.9, 124.2, 87.1, 71.9, 70.9, 70.0, 67.0, 61.2, 55.2, 40.7; **^{19}F-NMR** (376 MHz, CD_3CN) δ -72.8 (d, *J* = 708 Hz); **^{31}P-NMR** (162 MHz, CD_3CN) δ -144.6 (sept., *J* = 708 Hz); **MS** (ESI +ve) *m/z* 563.0153 ($[M]^{2+}$, $C_{50}H_{44}O_2N_6I_2Fe_2$, calc. 563.0152).

Ferrocene-appended HB Receptor **2.HB**

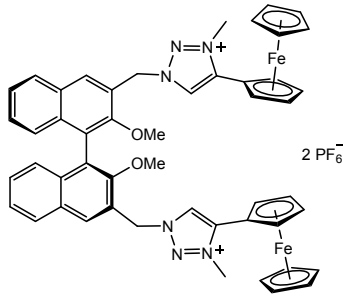

Quantities of reagents used: **8.HB** (30 mg, 0.036 mmol), trimethyloxonium tetrafluoroborate (11 mg, 0.075 mmol). Purification was achieved using preparatory thin layer chromatography (7 % MeOH in CH_2Cl_2 as eluent). Following anion exchange, **1.XB** was obtained as an orange solid (31 mg, 75 %). **^{1}H-NMR** (400 MHz, d_6-acetone) δ 8.92 (2H, s, triazolium-*H*), 8.33 (2H, s, Ar*H*), 8.03 (2H, d, ^3J = 6.8 Hz, Ar*H*), 7.50 (2H, t, ^3J = 6.4 Hz, Ar*H*), 7.36 (2H, t, ^3J = 6.4 Hz, Ar*H*), 7.16 (2H, d, ^3J = 6.4 Hz, Ar*H*), 6.12 (4H, m, CH_2-triazolium), 4.93 (4H, m, Fc*H*), 4.60 (4H, s, Fc*H*), 4.42 (6H, s, iodotriazolium-CH_3), 4.23 (10H, s, Fc*H*), 3.31 (6H, s, OCH_3); **^{13}C-NMR** (100 MHz, d_6-acetone) δ 154.6, 144.3, 135.1, 132.7, 130.3, 128.7, 127.9, 127.3, 125.8, 125.6, 125.4, 123.7, 71.4, 70.2, 68.9, 65.9, 60.3, 54.0, 39.0; **^{19}F-NMR** (376 MHz, d_6-acetone) δ -72.3 (d, *J* = 708 Hz); **^{31}P-NMR** (162 MHz, d_6-acetone) δ -144.4 (sept., *J* = 708 Hz); **MS** (ESI +ve) *m/z* 437.1195 ($[M]^{2+}$, $C_{50}H_{46}O_2N_6I_2$, calc. 437.1185).

Preparation of chiral tetrabutylammonium (TBA) salts of anions

The method reported by Huszthy and co-workers was employed.[4]

The appropriate commercially-available *N*Boc-amino acid or BINOL-PO_4H (1.0 eqv.) was mixed with methanol methanol (1.0 mL) and cooled to 0 °C. To this solution was added a 1.0 M methanolic solution of TBA hydroxide (1.0 eqv.) dropwise and stirred for 1 hour. The solvent was then removed *in vacuo* and the product dried on a high vacuum for 3 days before usage. The hygroscopic TBA salts were stored in a vacuum dessicator between usage.

S2. Spectral Characterisation of (*S*)-BINOL Receptors

Receptor **1.XB**

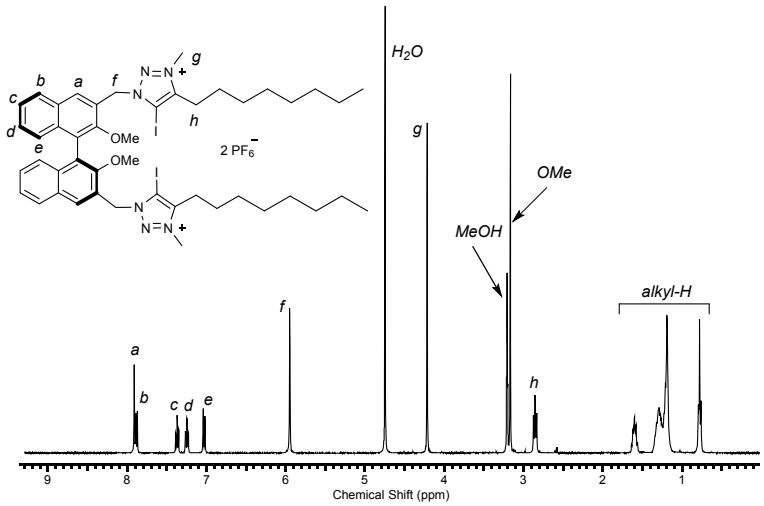

Figure S2-1. ^{1}H NMR of receptor **1.XB** in CD_3OD at 298 K (400 MHz).

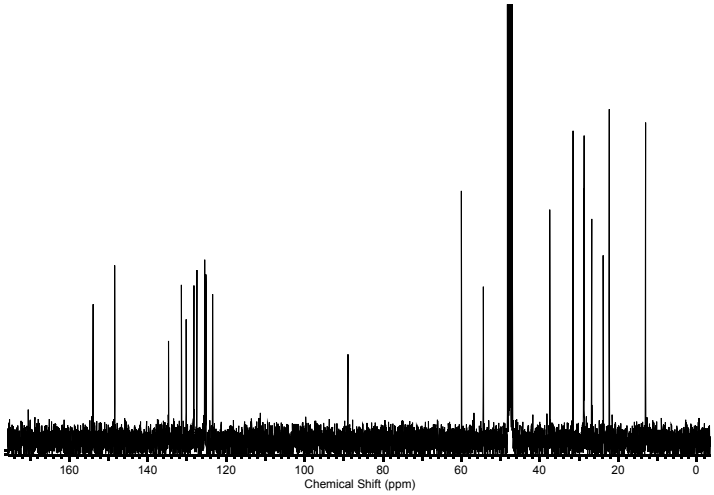

Figure S2-2. ^{13}C NMR of receptor **1.XB** in CD_3OD at 298 K (100 MHz).

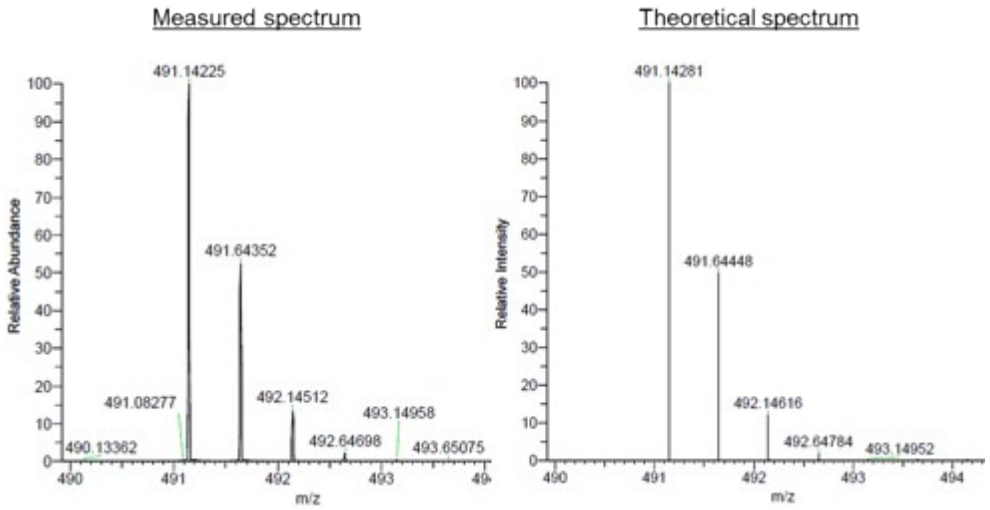

Figure S2-3. High-resolution ESI mass spectrum of **1.XB** (left) and its theoretical calculated spectrum (right).

Receptor **1.HB**

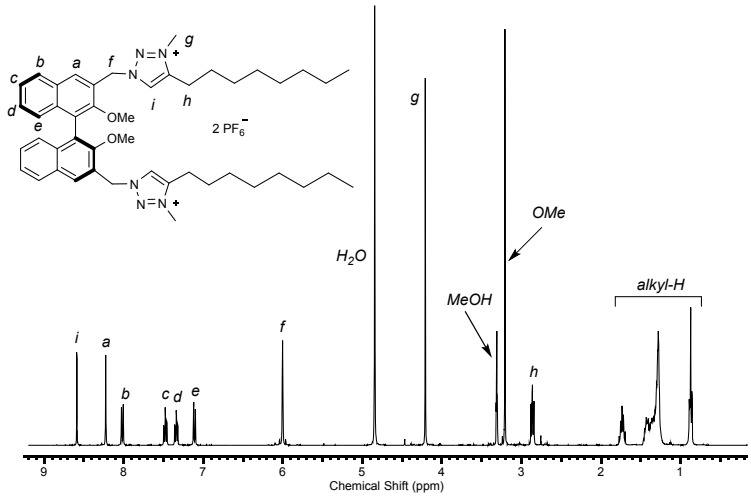

Figure S2-4. ^{1}H NMR of receptor **1.HB** in CD_3OD at 298 K (400 MHz).

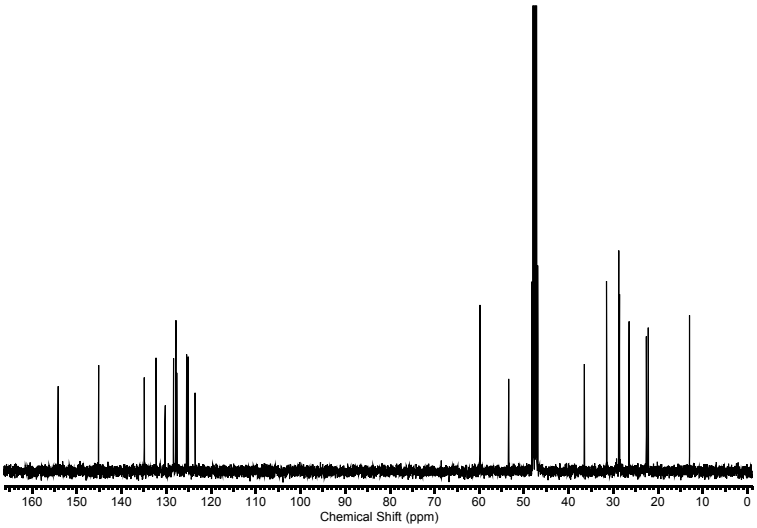

Figure S2-5. ^{13}C NMR of receptor **1.HB** in CD_3OD at 298 K (100 MHz).

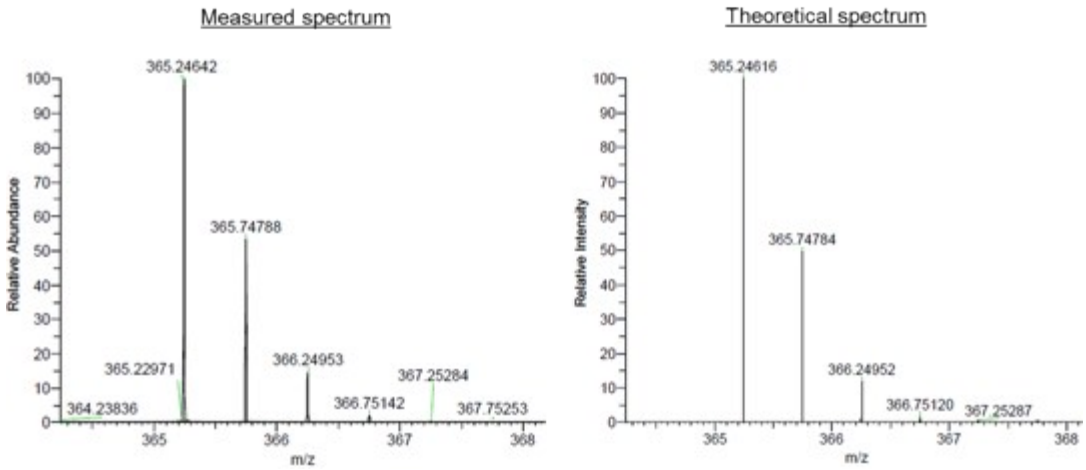

Figure S2-6. High-resolution ESI mass spectrum of **1.HB** (left) and its theoretical calculated spectrum (right).

Receptor **2.XB**

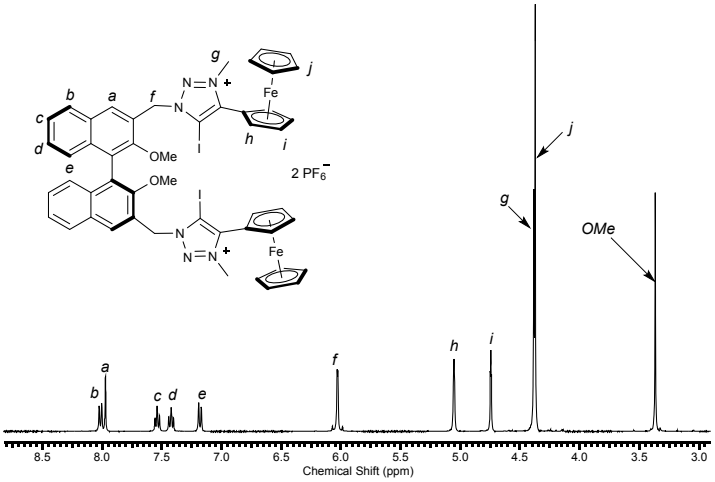

Figure S2-7. ^{1}H NMR of receptor **2.XB** in CD_3CN at 298 K (400 MHz).

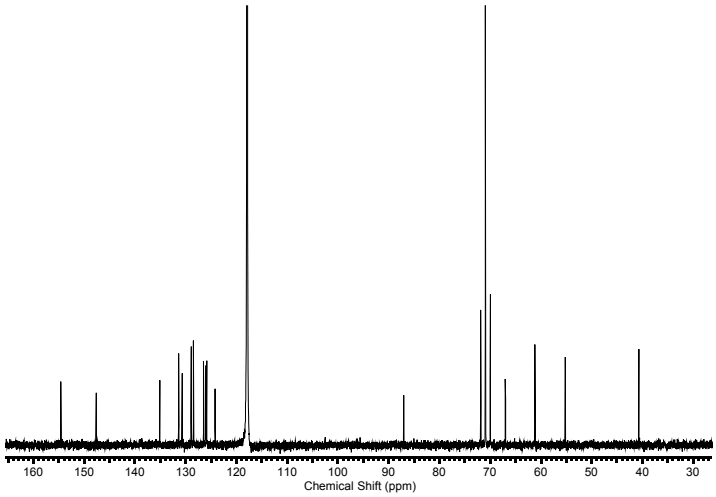

Figure S2-8. ^{13}C NMR of receptor **2.XB** in CD_3CN at 298 K (100 MHz).

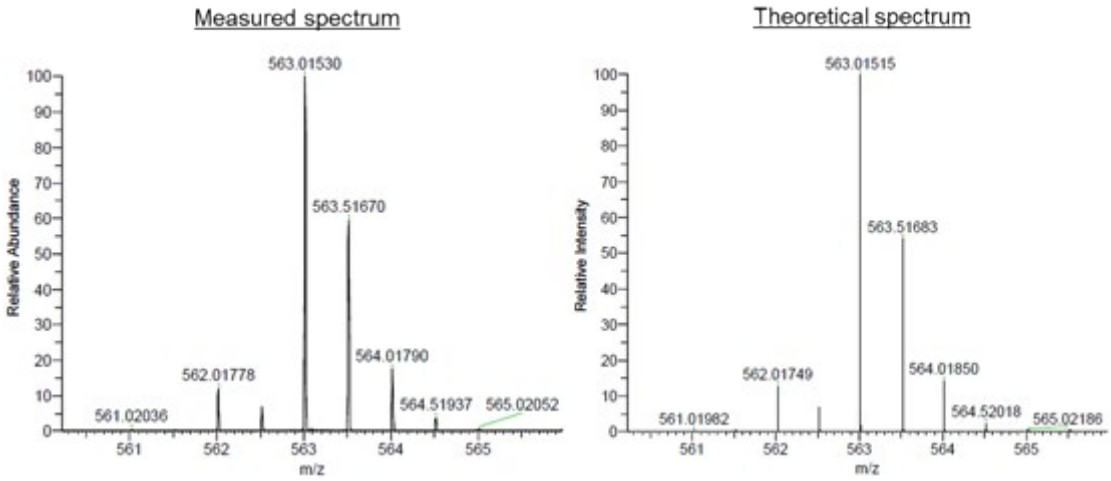

Figure S2-9. High-resolution ESI mass spectrum of **2.XB** (left) and its theoretical calculated spectrum (right).

Receptor **2.HB**

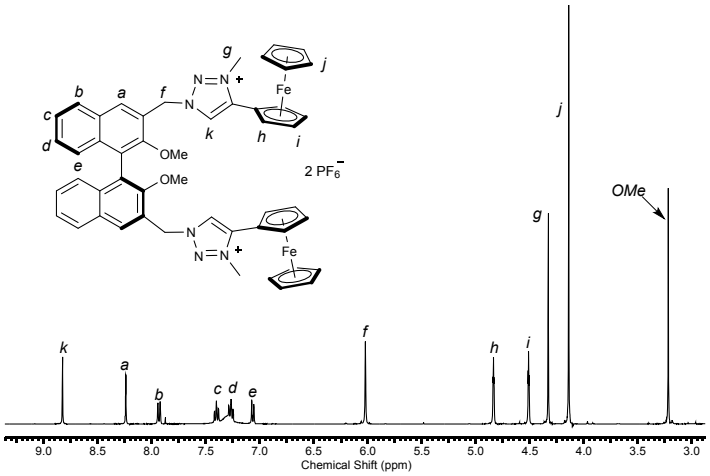

Figure S2-10. ^{1}H NMR of receptor **2.HB** in d_6-acetone at 298 K (400 MHz).

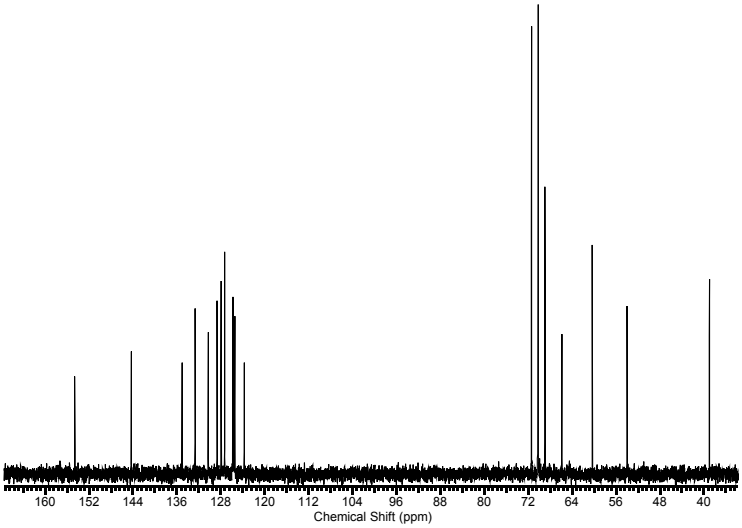

Figure S2-11. ^{13}C NMR of receptor **1.HB** in d_6-acetone at 298 K (100 MHz).

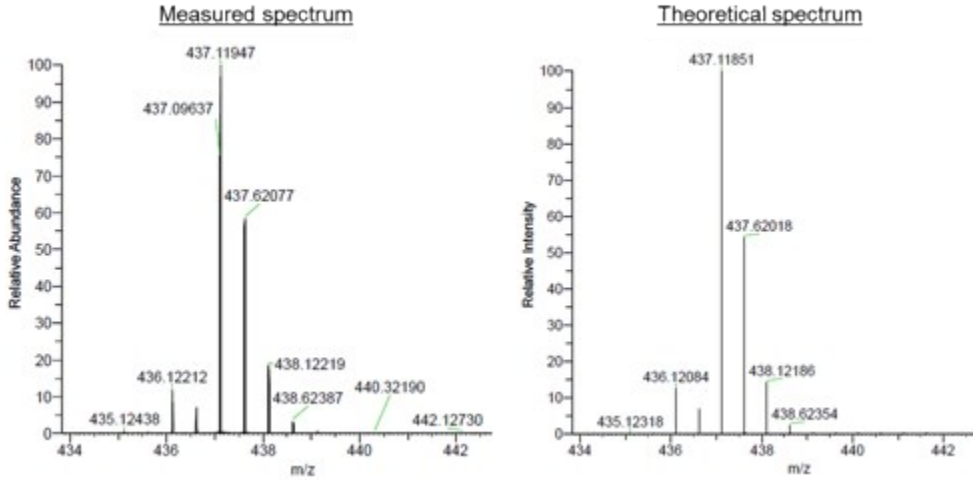

Figure S2-12. High-resolution ESI mass spectrum of **1.XB** (left) and its theoretical calculated spectrum (right).

S3. Anion Recognition Studies of Redox-active Receptors by ^{1}H NMR titrations

S3.1 General Titration Protocol

^{1}H NMR titration experiments were performed on a Bruker AVIII 500 MHz spectrometer. In a typical experiment, a solution of the appropriate tetrabutylammonium (TBA) salt was added to the receptor solution at 298 K. Both TBA salt and receptor were dissolved in the CD_3CN/D_2O 99:1. TBA was chosen as the counter-cation due to its non-coordinating nature. For all receptors, the binding of anions was found to be fast on the NMR timescale. The values of the observed chemical shift and concentration of anion were entered into the WinEQNMR2 computer programme[5] for every titration point. From initial estimates made of the binding constants (*K*) and limiting chemical shifts, these parameters were refined using non-linear least-squares analyses to obtain the best fit between empirical and calculated chemical shifts using a 1:1 binding stoichiometry. The input parameters were varied till convergence of the best fit values of the binding constants and their errors were obtained. In all cases, a 1:1 host-guest binding model gave the best fit for the experimental data, with errors ($\pm$) obtained being smaller than 10 % of the *K* value calculated. For all subsequent binding isotherms presented in the following pages, empirical data points are represented by the filled dots, while continuous lines represent the calculated binding curves.

A 0.075 M solution of the TBA salts for *N*Boc-alanine and *N*Boc-leucine was added to 0.50 mL of a 1.5 mM solution of receptor, where 1.0 equivalent of salt added corresponds to 10 μL of the salt solution. Due to poorer solubility of TBA(*N*Boc-tryptophan) and TBA(BINOL-PO_4) in the solvent mixture, a 0.0375 M solution of the salts were used instead, where 20 μL of the salt solution corresponded to 1.0 equivalent of salt added. For the receptors **1.XB** and **2.XB**, the chemical shift of the signal for H_e (Figure S3-1) were monitored for 17 data points corresponding to 0.0, 0.2, 0.4, 0.6, 0.8, 1.0, 1.2, 1.4, 1.6, 1.8, 2.0, 2.5, 3.0, 4.0, 5.0, 7.0 and 10.0 equivalents of added guest anion. For **1.HB**, as no perturbations of H_e were observed during the titration, the proto-triazolium protons (H_i in Figure S2-4) were monitored instead. Due to weaker binding, an additional data point corresponding to 15.0 equivalents of anion (total of 18 data points) was obtained during the titrations to ensure sufficient plateauing of the binding isotherms for reliable binding constants to be obtained.

S3.2 Assigning Aromatic ^{1}H NMR Signals Receptor 1.XB

As shown from the ^{1}H NMR spectrum of **1.XB** (Pg S9), the signals (doublets) corresponding to H_b and H_e cannot be unambiguously distinguished from the spectra alone. As the singlet signal arising from H_a does not overlap with other signals, and is expected to exhibit a NOE with H_b due to their spatial proximity (Figure S3-1), one-dimensional (1D) NOESY was performed. The resonant frequency corresponding to the signal for H_a was selectively pulsed, and as shown in Figure S3-1 below, a strong interaction was only observed with the peak for H_b. Due to the similarity of the ^{1}H NMR spectra corresponding to all the (*S*)-BINOL-derived receptors, this assignment applies for them as well.

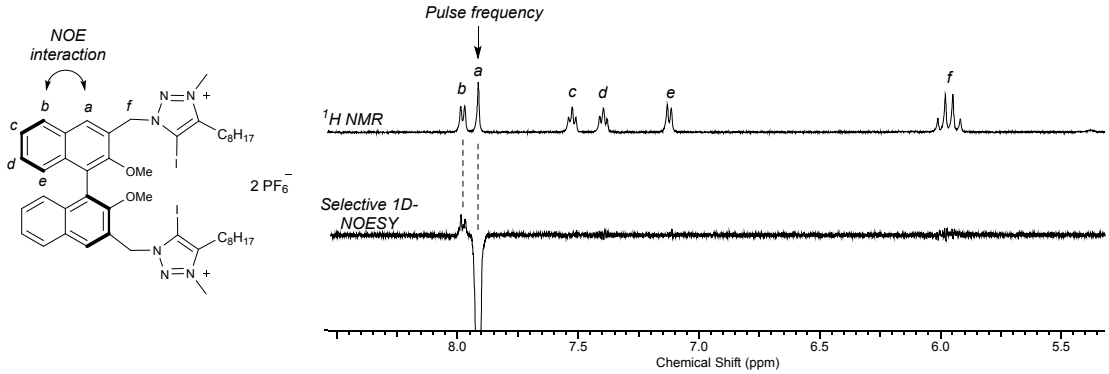

Figure S3-1. Partial ^{1}H NMR and one-dimensional (1D) selective NOESY spectra of **1.XB** (500 MHz, CD_3CN/ D_2O 99:1, 298 K).

S3.3 ^{1}H NMR titration data

Receptor **1.XB**

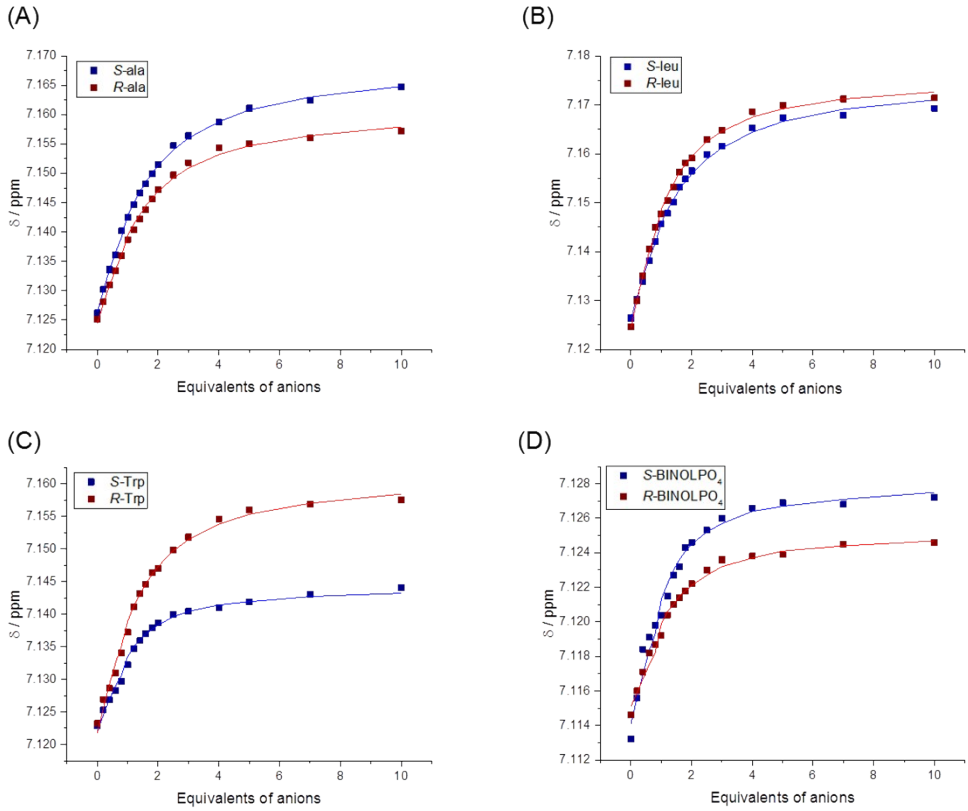

Figure S3-2. Plot of chemical shift of the signal corresponding to H_e (assignment in Figure S3-1) against equivalents of (A) *N*Boc-alanine; (B) *N*Boc-leucine; (C) *N*Boc-tryptophan and (D) BINOL-PO_4 added in CD_3CN/D_2O 99:1 ([host] = 1.5 mM, 500 MHz, T = 298 K).

Receptor **1.HB**

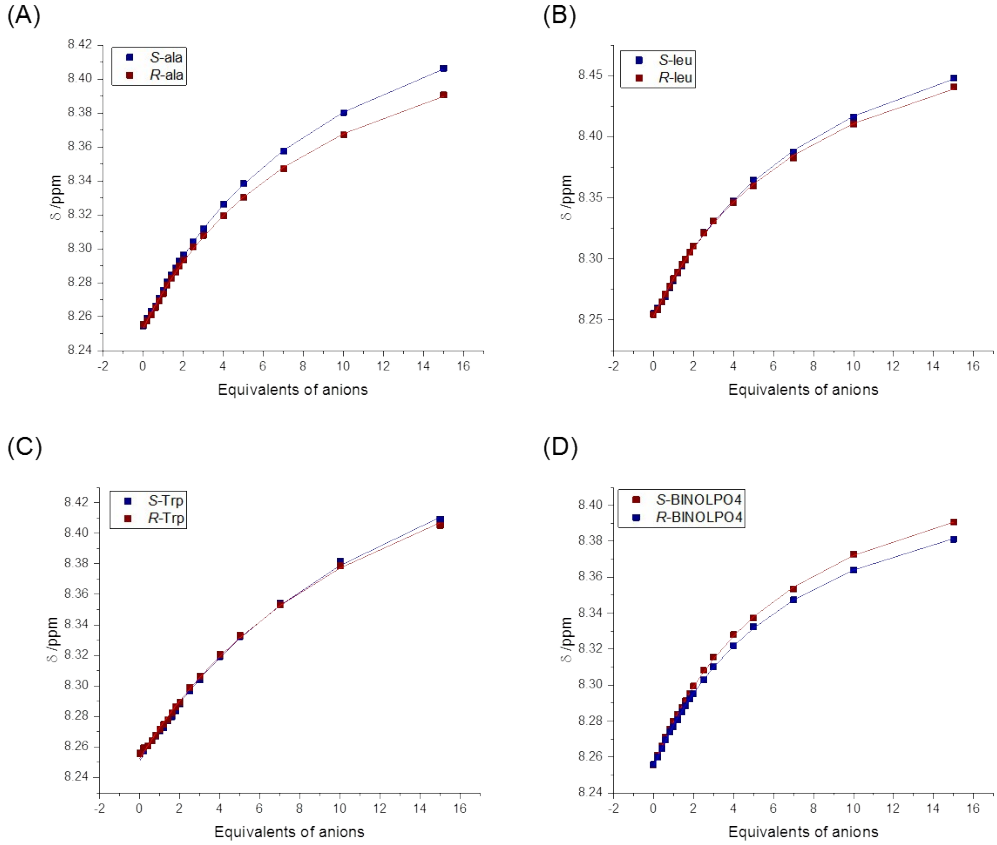

Figure S3-3. Plot of chemical shift of the signal corresponding to triazolium-*H* against equivalents of (A) *N*Boc-alanine; (B) *N*Boc-leucine; (C) *N*Boc-tryptophan and (D) BINOL-PO_4 added in CD_3CN/D_2O 99:1 ([host] = 1.5 mM, 500 MHz, T = 298 K).

Receptor **2.XB**

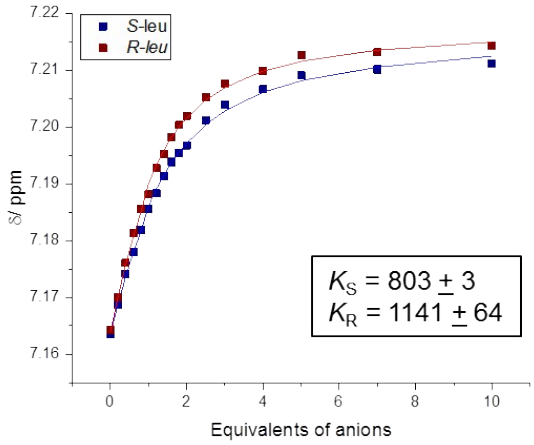

Figure S3-4. Plot of chemical shift of the signal corresponding to H_e against equivalents of (A) *N*Boc-alanine; (B) *N*Boc-leucine; (C) *N*Boc-tryptophan and (D) BINOL-PO_4 added in CD_3CN/D_2O 99:1 ([host] = 1.5 mM, 500 MHz, T = 298 K).

S4. Electrochemical Studies

S4.1 General Protocol

All electrochemical studies were performed on an Autolab PGSTAT-12 system and all data was analysed using General Purpose Electrochemical Software (GPES) version 4.9. All electrochemistry was performed using a standard 3 electrode cell in a Faraday cage, and undertaken in anhydrous acetonitrile with 0.1 M $TBAPF_6$ supporting electrolyte. All diffusive voltammetry was undertaken at a 3 mm diameter glassy carbon working electrode (BASi), cleaned prior to use using 0.3 micron alumina powder (Buehler), and all potentials were referenced to a $Ag/AgNO_3$ reference electrode;[6] the latter was prepared using an anhydrous acetonitrile-based solution of 10 mM $AgNO_3$ and 0.15 M $TBAPF_6$. A $Ag/AgNO_3$ reference electrode was used in preference to the more commonly used Ag/AgCl reference electrode in order to prevent any potential interference in the sensory response of the receptors arising from any chloride anion leakage. All solutions were degassed with dry nitrogen prior to the recording of each CV/ SWV. CVs were recorded with a 1 s equilibration time, step potential of 1 mV and at a scan rate of 100 mV s^{-1}. For all the host systems investigated, the host was dissolved in the electrolyte solution to afford a concentration of 0.5 mM. The electrochemical reversibility of each system was probed by varying the CV scan rate.

Electrochemical anion binding experiments were performed using square-wave voltammetry (SWV). SWVs were typically recorded with a 1 s equilibration time, a step potential of 3 mV and a frequency of 30 Hz. The titrations were performed by adding known aliquots of anions to a 1.5 mL solution of receptor in the same electrolyte mixture corresponding to 0.0, 0.5, 1.0, 2.0, 3.0 and 5.0 equivalents respectively. Higher equivalents of anion were not used due to the loss of SWV peak current observed.

S4.2 Electrochemical Reversibility Studies

The electrochemical reversibility of our host systems are probed by recording CV scans at different scan rates. An electrochemical system is described as reversible, and hence exhibits fast electron transfer kinetics, when the following criteria are met:

1. ΔE_p = (59 / n) mV, where n = number of electrons transferred in the redox process. For our ferrocene-appended host systems, n = 1 during ferrocene redox chemistry. Hence, ΔE_p should be 59 mV for our systems.
2. Potentials E_{pa} and E_{pc} corresponding to peak oxidation and reduction currents respectively are independent of the scan rate.
3. The peak cathodic (I_{pc}) and anodic (I_{pa}) currents are of equal magnitude, i.e. $I_{pc} / I_{pa} = 1$.

Unless otherwise stated, all CVs are recorded in 0.1 M $TBAPF_6$ electrolyte solution in acetonitrile and potentials are compared to the $Ag / AgNO_3$ reference electrode.

Receptor **2.XB**

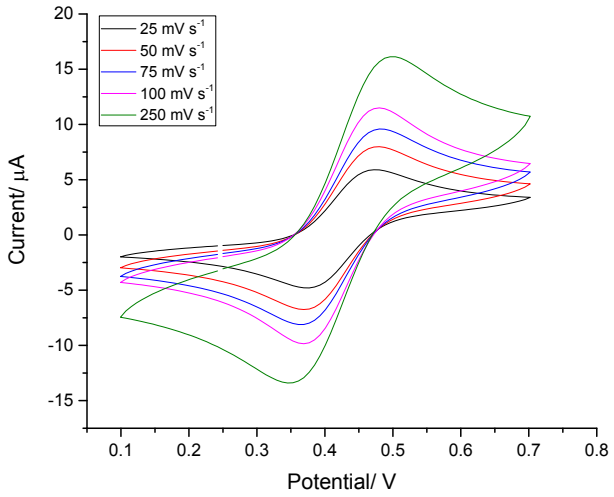

Figure S4-1. CVs of receptor **2.XB** at different scan rates ([host] = 0.5 mM, T = 293 K).

Table S4-1. Values of E_{pc}, E_{pa}, I_{pa}, I_{pc} ΔE_p and I_{pa}/ I_{pc} for **1.XB** recorded at different scan rates.

Scan rate/ mV s^{-1}	E_{pa}/V	E_{pc}/V	I_{pa}/ µA	I_{pc}/ µA	ΔE_p / V	I_{pa} / I_{pc}
25	0.480	0.369	4.73	5.03	0.111	0.94
50	0.480	0.369	6.34	6.79	0.111	0.93
75	0.480	0.369	7.46	7.96	0.111	0.94
100	0.480	0.369	9.14	9.79	0.111	0.93
250	0.496	0.345	11.52	12.25	0.151	0.94

From the reversibility studies, receptor **2.XB** is best described as displaying a quasi-reversible Fc/Fc^+ redox couple.

Receptor **2.HB**

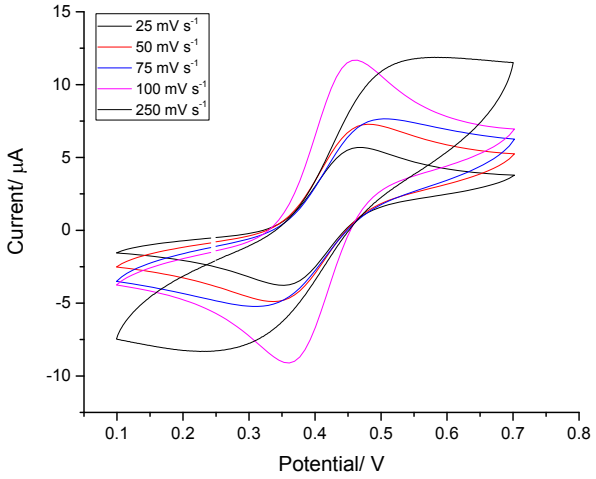

Figure S4-2. CVs of receptor **2.HB** at different scan rates ([host] = 0.5 mM, T = 293 K).

Table S4-2. Values of E_{pc}, E_{pa}, I_{pa}, I_{pc} ΔE_p and I_{pa}/ I_{pc} for **1.XB** recorded at different scan rates.

Scan rate/ mV s^{-1}	E_{pa}/V	E_{pc}/V	I_{pa}/ µA	I_{pc}/ µA	ΔE_p / V	I_{pa} / I_{pc}
25	0.464	0.353	4.13	4.16	0.111	0.99
50	0.488	0.329	4.69	4.59	0.159	1.02
75	0.504	0.313	6.42	7.12	0.191	0.90
100	0.464	0.361	9.13	9.41	0.103	0.97
250	0.557	0.276	-[a)]	-[a)]	0.281	-[a)]

[a)] Not possible to accurately determine values of I_{pa} and I_{pc} from the CV obtained.

From the large fluctuations of ΔE_p and I_{pa} / I_{pc} at different scan rates, and the poorly-defined CV obtained at a scan rate of 250 mV s^{-1}, receptor **2.HB** can be described as having poor electrochemical reversibility. Hence, it was not used for further sensing studies.

S4.3 Data for Electrochemical Anion titrations in Dry Acetonitrile

The concentration of the TBA(*N*Boc-alanine) and TBA(*N*Boc-leucine) stock solutions used for titrations was 150 mM, where 5.0 µL of anion corresponded to 1.0 equivalents. Due to poorer solubility in acetonitrile, 37.5 mM solutions of TBA(*N*Boc-tryptophan) and TBA(BINOL-PO_4) were prepared where 20.0 µL of anion solution corresponded to 1.0 equivalents.

Receptor **2.XB**

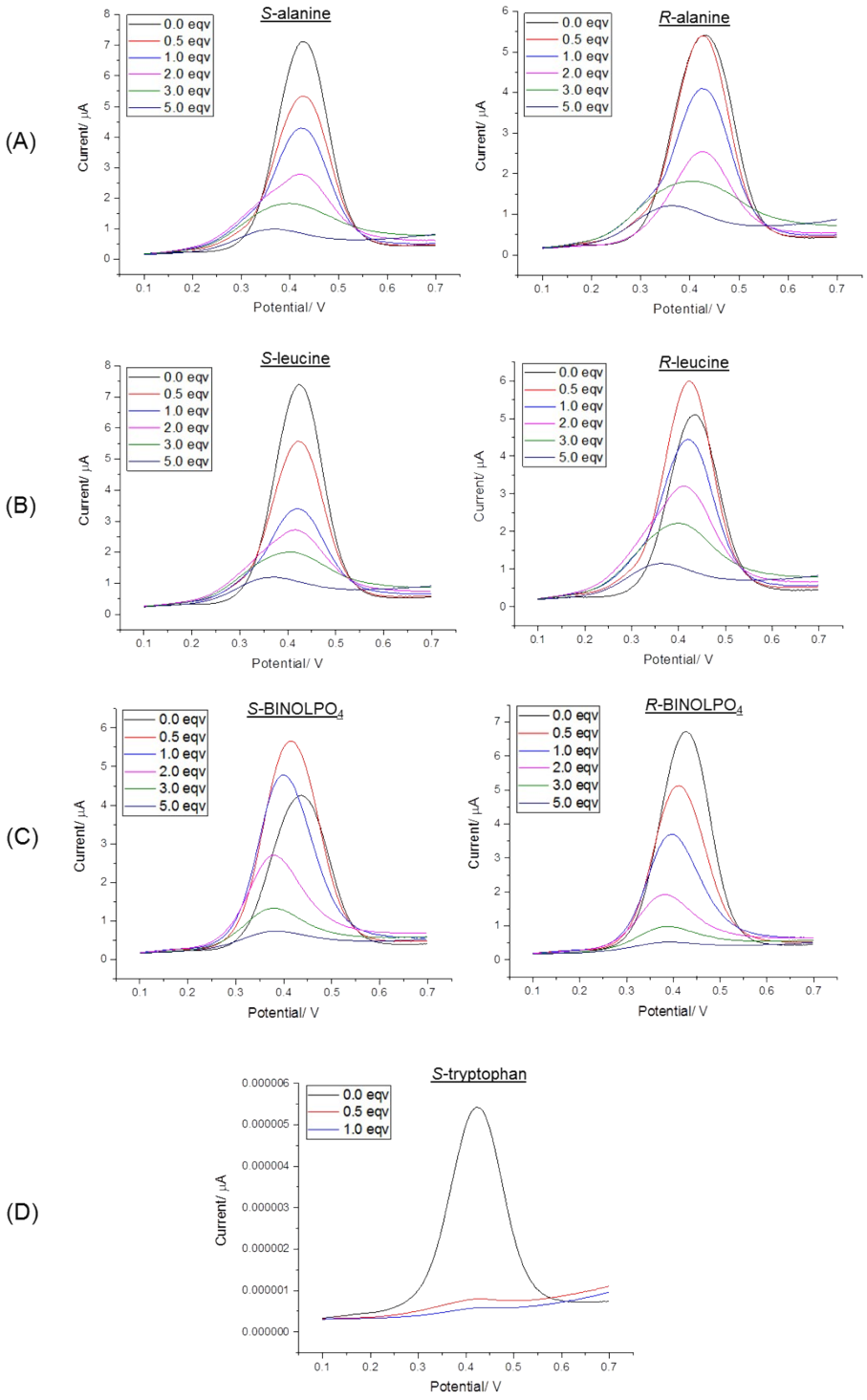

Figure S4-3. SWVs of receptor **2.XB** upon the addition of both enantiomers of (A) TBA(*N*Boc-alanine); (B) TBA(*N*Boc-leucine), (C) TBA(BINOL-PO_4) and (D) TBA(*N*Boc-tryptophan). For TBA(*N*Boc-tryptophan), no reliable electrochemical data could be obtained due to oxidation of the tryptophan moiety at anodic potentials[7] ([host] = 0.5 mM, T = 293 K).

S5. Computational Data

S5.1 Extended discussion of HB and XB interactions in MD simulations

These intermolecular interactions were monitored throughout the simulation time of all MD runs and are plotted in Figure S5-1 to Figure S5-4, together with the distance between the centre of mass defined by the two iodine atoms of **1.XB** and the centre of mass determined by the two pertinent oxygen atoms from the anionic substrate ($I_{COM,host}\cdots O_{COM,anion}$). Overall, **1.XB** maintains with the chiral substrates two continuous halogen bonds, with exception of 8/24 MD runs (3 *N*Boc-(*S*)-alanine; 1 *N*Boc-(*R*)-leucine; 1 *N*Boc-(*S*)-tryptophan; 1 *N*Boc-(*R*)-tryptophan; and 2 (*S*)-BINOL-PO_4) where a C-I$\cdots O_{anion}$ XB interaction is sporadically interrupted (orange line in Figures S5-1 to S5-4). Concomitantly, a new HO–H$\cdots O_{anion}$ hydrogen bond emerges (blue line) together with a C-I$\cdots OH_2$ halogen bonding interaction (purple line), leading to an increase of the $I_{COM,host}\cdots O_{COM,anion}$ distance (red line). In contrast, the HO–H$\cdots$I hydrogen bonds are undoubtedly in lesser number (green line) and seem to be interrupted when an XB interaction is formed with the water molecule.

S5.2 Additional figures

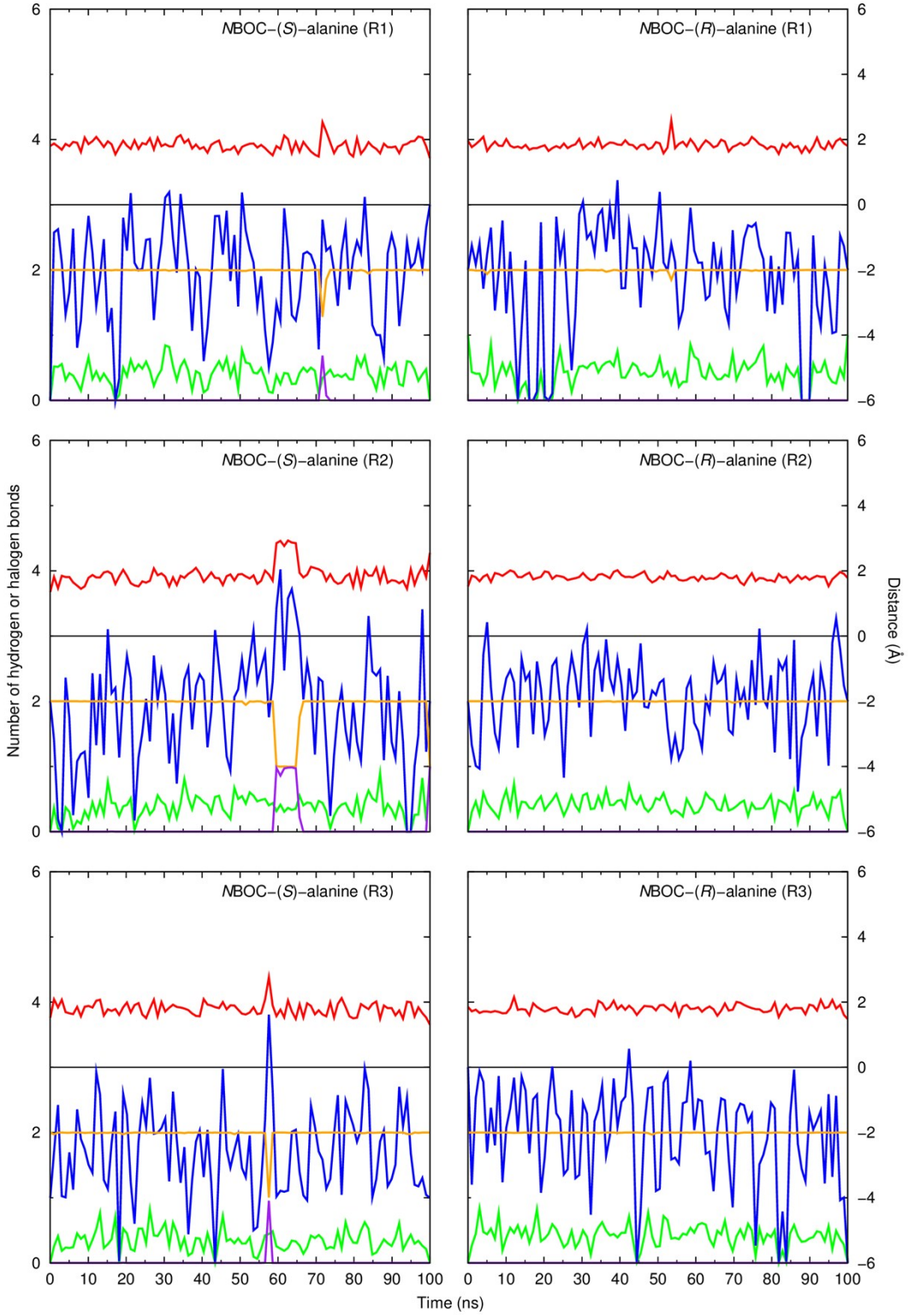

Figure S5-1. Evolution of the $I_{COM,host}\cdots O_{COM,anion}$ distance (red line) throughout 100 ns of independent MD runs, together with the number of HB interactions, HO–H$\cdots O_{anion}$ (blue line) and HO–H$\cdots$I (green line), and the number of XB interactions, C-I$\cdots OH_2$ (purple line) and C-I$\cdots O_{anion}$ (orange line), for the diastereoisomeric complexes of **1.XB**.

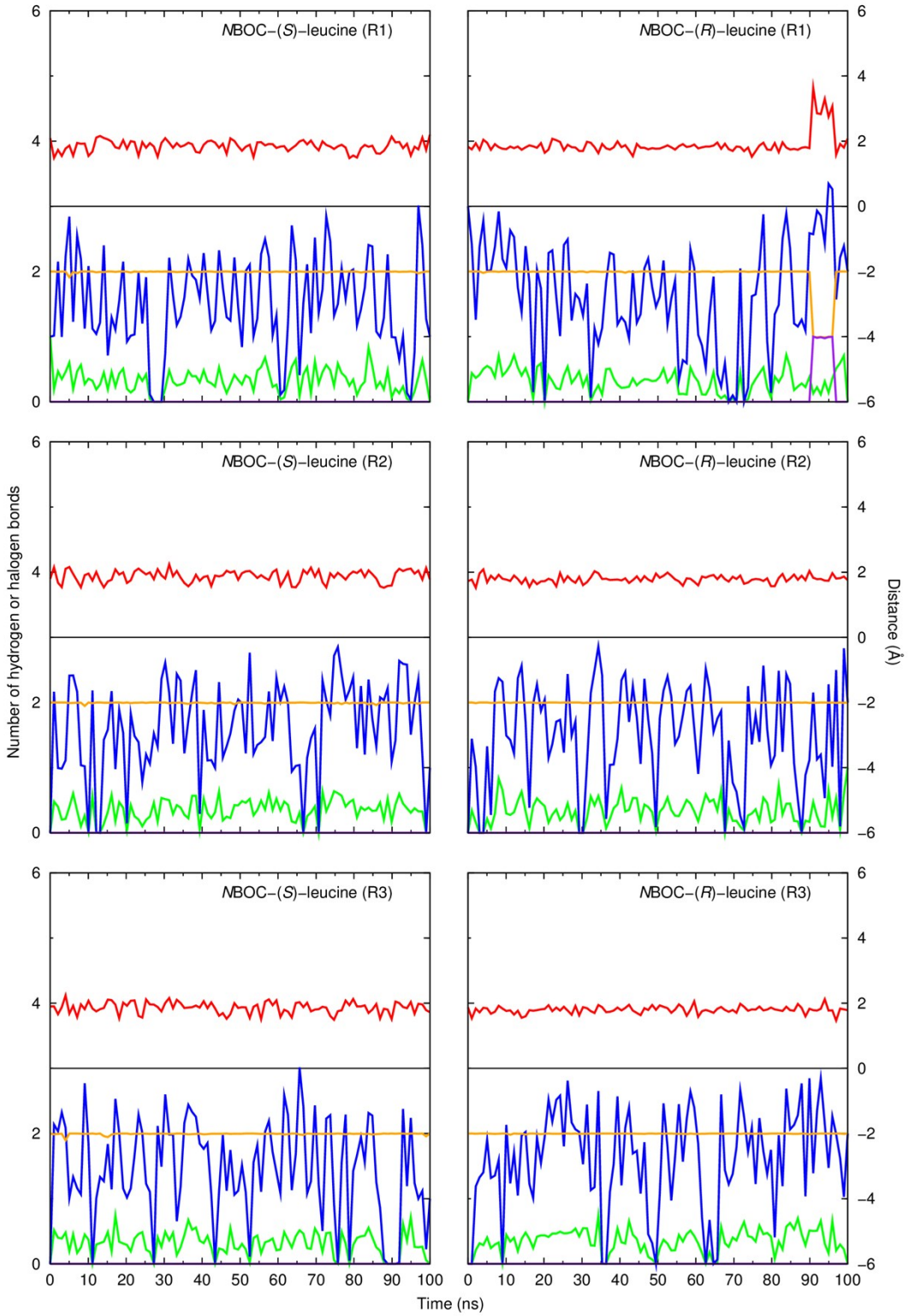

Figure S5-2. Evolution of the $I_{COM,host}\cdots O_{COM,anion}$ distance (red line) throughout 100 ns of independent MD runs, together with the number of HB interactions, HO–H$\cdots$$O_{anion}$ (blue line) and HO–H$\cdots$I (green line), and the number of XB interactions, C-I$\cdots$$OH_2$ (purple line) and C-I$\cdots$$O_{anion}$ (orange line), for the diastereoisomeric complexes of **1.XB**.

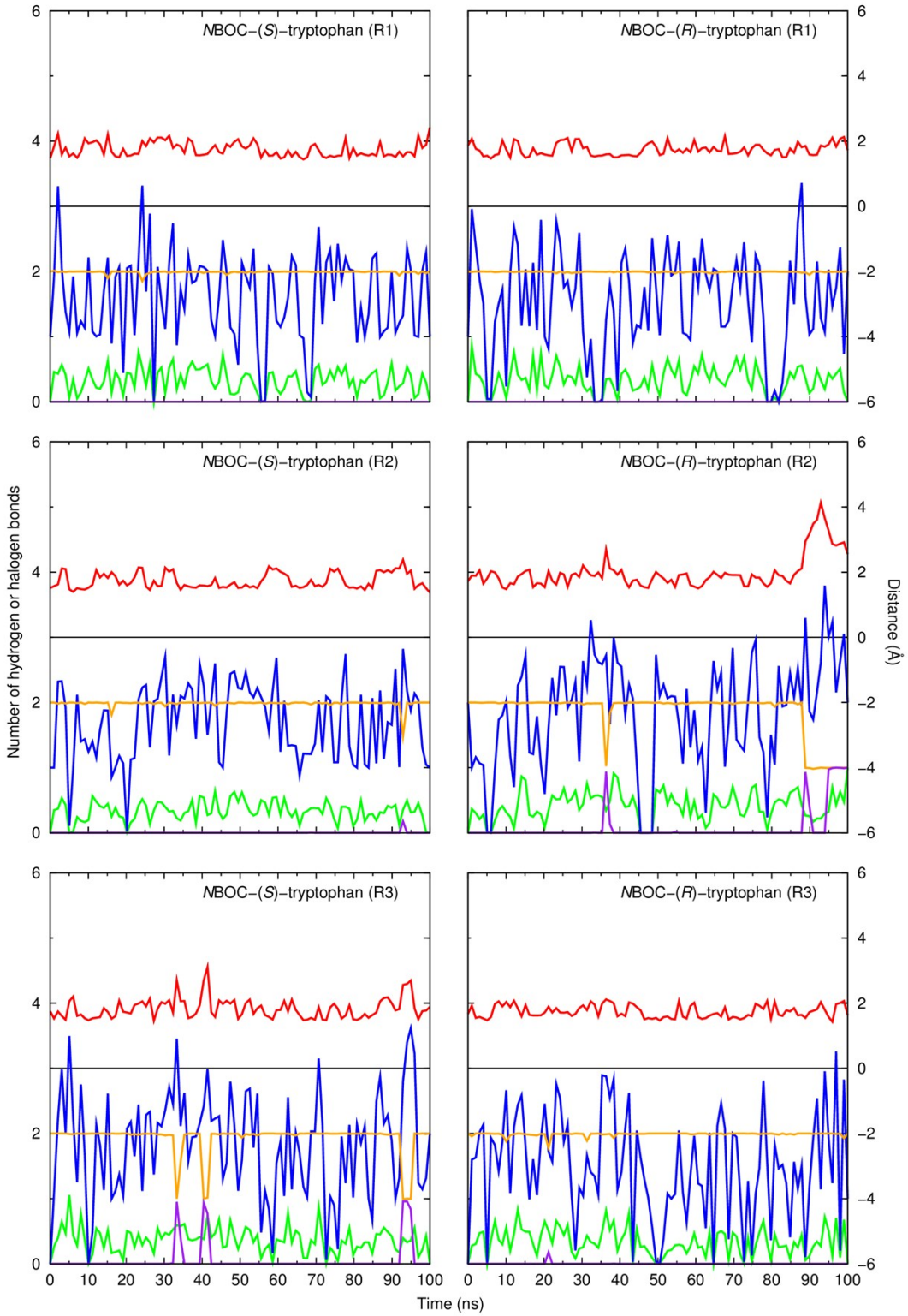

Figure S5-3. Evolution of the $I_{COM,host}\cdots O_{COM,anion}$ distance (red line) throughout 100 ns of independent MD runs, together with the number of HB interactions, HO–H$\cdots O_{anion}$ (blue line) and HO–H$\cdots$I (green line), and the number of XB interactions, C-I$\cdots OH_2$ (purple line) and C-I$\cdots O_{anion}$ (orange line), for the diastereoisomeric complexes of **1.XB**.

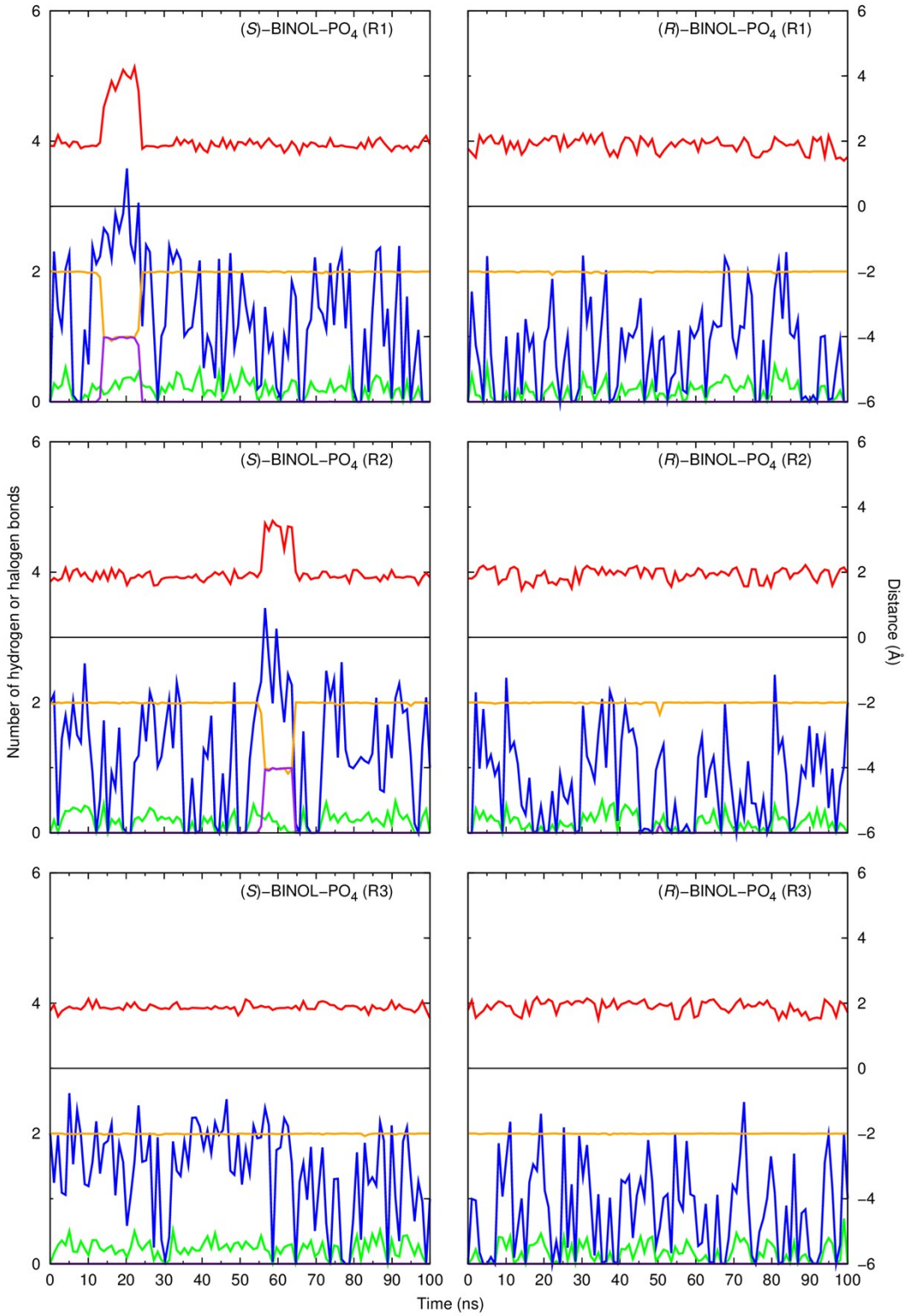

Figure S5-4. Evolution of the $I_{COM,host}\cdots O_{COM,anion}$ distance (red line) throughout 100 ns of independent MD runs, together with the number of HB interactions, HO–H$\cdots O_{anion}$ (blue line) and HO–H$\cdots$I (green line), and the number of XB interactions, C-I$\cdots OH_2$ (purple line) and C-I$\cdots O_{anion}$ (orange line), for the diastereoisomeric complexes of **1.XB**.

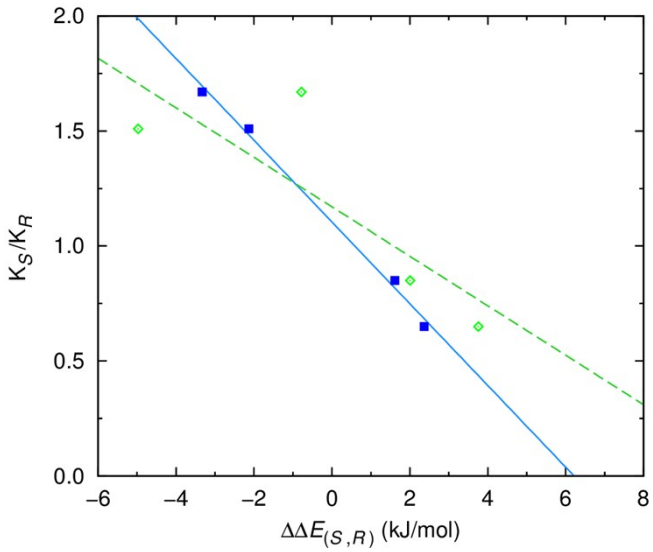

Figure S5-5. Plot of $\Delta\Delta E_{(S,R)}$ *vs* K_S/K_R for **1.XB** chiral complexes. The $\Delta\Delta E_{\text{bind}(S,R)}$ is shown in blue filled squares and $\Delta\Delta E_{\text{vdW}(S,R)}$ is shown in open green diamonds. The light blue line and the green dashed line correspond to the linear fitting of the blue squares or the green diamonds data, respectively.

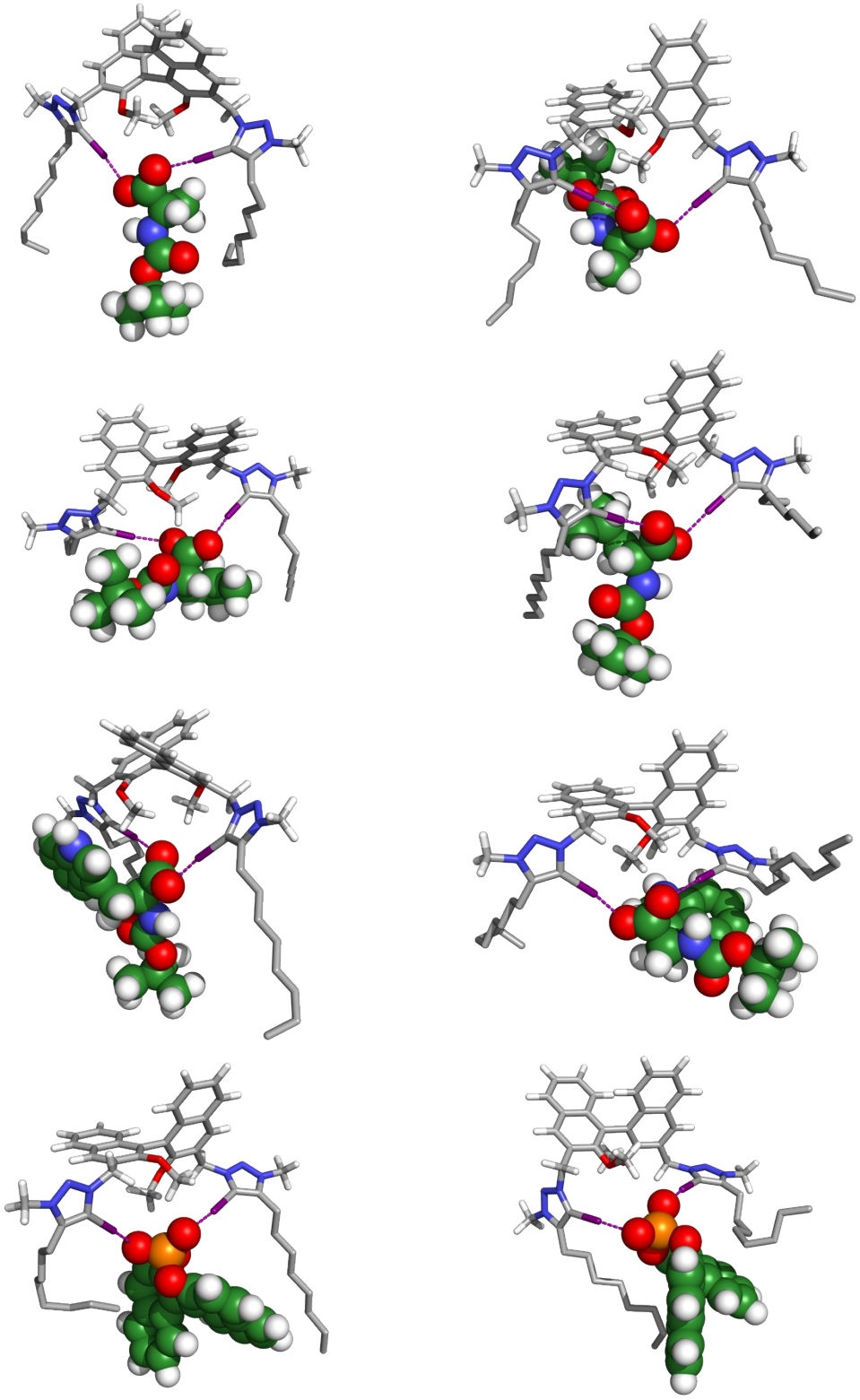

Figure S5-6. DFT optimised structures for complexes of **1.XB** with *N*Boc-alanine (first row), *N*Boc-leucine (second row) and *N*Boc-tryptophan derivatives (third row) or BINOL-PO_4 (bottom row), with the *S* enantiomers of the substrates shown on the left column and the *R* enantiomers shown on the right one. The receptor and the substrate are shown in sticks and in spheres, with the carbon atoms shown in grey and green, respectively. The oxygen, nitrogen, iodine, phosphorus and hydrogen atoms are shown in red, blue, purple, orange and white, in this order. The halogen bonds are shown as purple dashed lines. The C-H bonds on the octyl substituent are hidden for clarity.

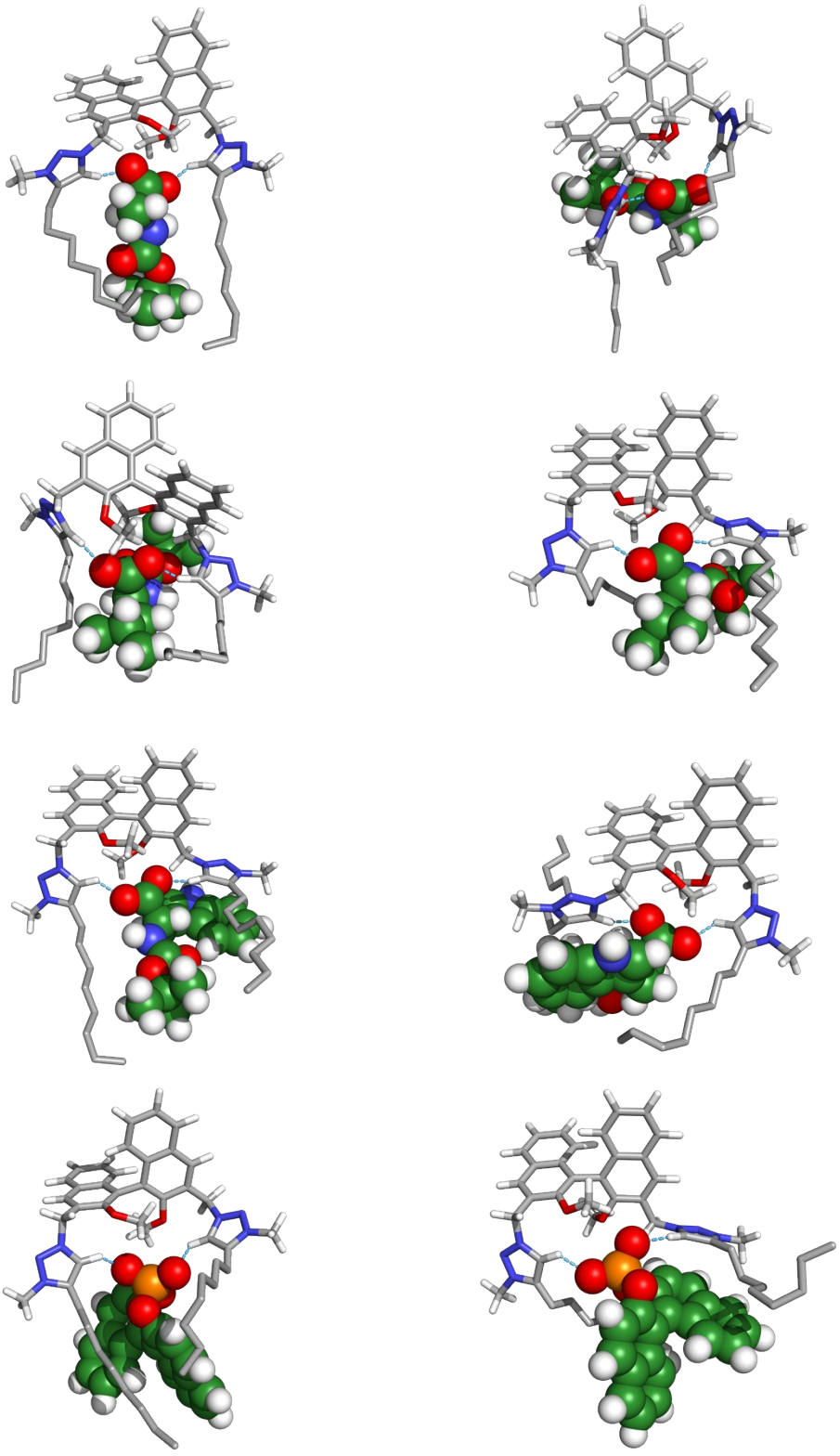

Figure S5-7. DFT optimised structures for complexes of **1.HB** with *N*Boc-alanine (first row), *N*Boc-leucine (second row) and *N*Boc-tryptophan derivatives (third row) or BINOL-PO_4 (last row), with the *S* enantiomers of the substrates shown on the left column and the *R* enantiomers shown on the right one. The hydrogen bonds are shown as light blue dashed lines. Remaining details as given in Figure S5-6.

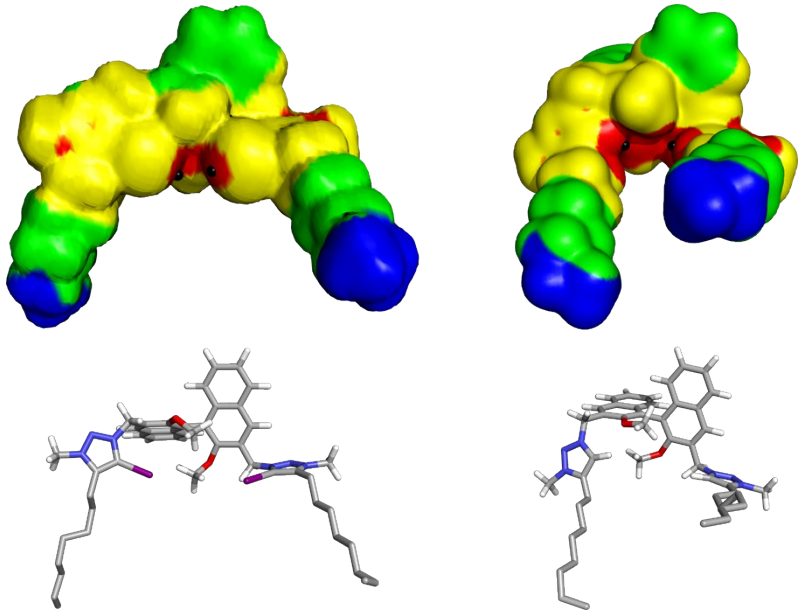

Figure S5-8. Distribution of the electrostatic potential onto the electron density surface (0.001 electrons per Bohr^3) of **1.XB** (top left) and **1.HB** (top right). These structures (shown in the bottom) were obtained after optimisation with *N*Boc-(*S*)-tryptophan and removal of the substrate. The colour ranges, in kJ/mol, are as follows: blue – below 263; green – between 263 and 394; yellow – between 394 and 526; red – above 526. The most positive values of each binding unit, $V_{S,max}$, are identified by black dots (612 and 606 kJ/mol for **1.XB**; 638 and 616 kJ/mol for **1.HB**), and correspond to the σ-holes on the iodine bis-triazolium substituents of **1.XB** or are located in the vicinity of pertinent hydrogen atoms of **1.HB**. Remaining details as given in Figures **S5-6** and **S5-7**.

S5.3 Additional tables

Table S5-1. Average molecular mechanics energies (kJ/mol) of the solvated diastereoisomeric complexes obtained from the molecular dynamics simulations,[a] along with $\Delta\Delta E_{bind(S,R)}$ energy differences.

Substrate	*S* enantiomer		*R* enantiomer		$\Delta\Delta E_{bind(S,R)}$
	Avg ± SD	*N*	Avg ± SD	*N*	
*N*Boc- Ala	-115966.70 ± 68.23	288000	-115968.32 ± 68.26	300000	1.61
*N*Boc- Leu	-116181.24 ± 68.44	300000	-116183.61 ± 68.29	293000	2.37
*N*Boc- Trp	-115925.12 ± 68.37	289000	-115921.78 ± 68.45	286000	-3.33
BINOL-PO_4	-115601.95 ± 68.46	279000	-115599.82 ± 68.15	300000	-2.13

[a] The values are the average over the three 100 ns MD simulations, apart the periods where complex disruption was observed; hence the *N* values lower than 300000 for some table entries.

Table S5-2. Distances (Å) and angles (°) between the binding units of **1.XB** or **1.HB** and substrates in the quantum optimised structures.

Receptor	Substrate	*S* enantiomer		*R* enantiomer	
		X···O[a]	C-X···O[a]	X···O[a]	C-X···O[a]
1.XB	*N*Boc- Ala	2.467 ; 2.488	171.4 ; 174.6	2.478 ; 2.454	177.1 ; 173.2
	*N*Boc- Leu	2.572 ; 2.424	173.6 ; 173.4	2.498 ; 2.491	172.2 ; 174.9
	*N*Boc- Trp	2.567 ; 2.465	171.6 ; 172.7	2.475 ; 2.683	171.6 ; 171.3
	BINOL-PO_4	2.491 ; 2.545	174.2 ; 175.1	2.553 ; 2.494	170.0 ; 174.2
1.HB	*N*Boc- Ala	2.019 ; 1.920	129.0 ; 143.0	2.193 ; 2.087	111.1 ; 120.6
	*N*Boc- Leu	1.934 ; 1.956	134.9 ; 145.0	2.039 ; 1.926	129.4 ; 146.1
	*N*Boc- Trp	1.957 ; 2.011	141.4 ; 129.1	2.124 ; 1.953	120.4 ; 151.1
	BINOL-PO_4	2.069 ; 1.856	122.4 ; 138.1	2.062 ; 1.978	123.6 ; 130.3

[a] X stands for I in **1.XB** receptor and for H in **1.HB**.

Table S5-3. Wiberg Bond Indices for the independent XB and HB interactions in the optimised diastereoisomeric complexes of **1.XB** and **1.HB**.

Substrate	**1.XB**		**1.HB**	
	S enantiomer	*R* enantiomer	*S* enantiomer	*R* enantiomer
*N*Boc- Ala	0.161 ; 0.144	0.145 ; 0.171	0.023 ; 0.041	0.014 ; 0.017
*N*Boc- Leu	0.102 ; 0.170	0.154 ; 0.138	0.034 ; 0.030	0.025 ; 0.042
*N*Boc- Trp	0.110 ; 0.173	0.165 ; 0.074	0.035 ; 0.025	0.016 ; 0.040
BINOL-PO_4	0.128 ; 0.110	0.121 ; 0.119	0.019 ; 0.033	0.017 ; 0.024

S5.4 Supplementary MD Movie Caption

Video S1. Movie of the third MD simulation of **1.XB**·*N*Boc-(*S*)-tryptophan (between the 91st the 96th ns). Four water molecules solvate the binding region and compete with the substrate for the binding units. The TBA and PF_6^- counter-ions, as well as the acetonitrile solvent molecules, are omitted for clarity. The receptor is shown in sticks and the chiral substrate in spheres, with C atoms shown in grey and green, respectively. O, N, I and H atoms are shown in red, blue, purple and white. The water molecules are shown in ball and sticks. The XB interactions are depicted as purple dashes. The octyl C-H bonds of **1.XB** are hidden for clarity.

S6. Computational Methods

S6.1 Starting structures for chiral substrates and receptors

Starting structures of receptors **1.XB** and **1.HB** and anionic substrates were generated through appropriated atomic manipulations of crystal structures deposited with the Cambridge Crystallographic Data Centre (CCDC).[8] The **1.XB** and **1.HB** with *S* chirality on the BINOL fragment were constructed from the crystal structure with Refcode GEMZUU,[9] while the the *N*Boc-(*S*)-alanine, *N*Boc-(*S*)-leucine, *N*Boc-(*R*)-tryptophan and (*R*)-binol-phosphate substrates were obtained from the crystal structures with Refcodes NASQAZ,[10] FAYMEZ,[11] DIZNEG,[12] and SORREX,[13] in that order. The atomic coordinates of other enantiomers were obtained by inversion of the crystal structures of their counterparts with Mercury CSD 3.6.[14-17]

S6.2 Quantum calculations

Overall, the quantum calculations carried out for this work were composed of geometry optimisations, distribution of electrostatic potential on the molecular surfaces **1.XB** and **1.HB**, derivatisation of restrained electrostatic potential (RESP) charges for **1.XB** and **1.HB** and the chiral substrates and natural bond orbital calculations (NBO). All quantum calculations were carried out using the Gaussian09 software,[18] unless stated otherwise.

Density functional theory (DFT) calculations were also employed in the parameterisation of the XB interactions using model complexes, as described in Section S6.4. The RESP charges were obtained from single point calculations undertaken with Hartree-Fock (HF) method using previously optimised structures (as detailed below), the Gaussian IOp(6/33=2, 6/41=4, 6/42=6) and the 6-31G* basis set for all atoms, except for the iodine atoms, in agreement with the GAFF development.[19, 20] In all calculations, the iodine atoms were described with the aug-cc-pVDZ-PP basis set,[21, 22] obtained from the EMSL website[23, 24]

S6.3 Classical force field calculations

All Molecular Mechanics (MM) and Molecular dynamics (MD) simulations were undertaken with Amber14.[25] The substrates and the tetrabutylammonium (TBA) counter-ion were described with default parameters taken from the Generalized Amber Force Field (GAFF)[19, 20] and RESP charges,[26] while the hexafluorophosphate (PF_6^-) was described with parameters and charges taken from ref. 27. The receptors **1.XB** and **1.HB** were also described with default GAFF parameters, apart the triazolium moiety, which was parameterised using quantum mechanics structural data, as detailed in Section 6.6. The solvent mixture was described with the TIP3P model for the water molecules, while the acetonitrile molecules were described with parameters and atomic charges taken from ref. 28. The structural data from MD simulations were obtained by post-processing of trajectory files with *cpptraj*.[29]

S6.4 Parameterisation of XB interactions

The force field parameterisation of the XB interactions was preceded by DFT optimisations of model complexes with acetate (CH_3COO^-) or dihydrogen phosphate ($H_2PO_4^-$), as archetypes of the binding units for chiral substrates *N*Boc-protected amino acids and BINOL-PO_4, respectively. In these model complexes, the octyl chains of **1.XB** were replaced by ethyl groups leading to $\mathbf{1.XB_{ethyl}}$ as model of

1.XB. These optimisations were carried using the B3LYP functional, with the H, C, N, O and P atoms treated with the 6-31+G* basis set, while the iodine atoms were described with the aug-cc-pVDZ-PP basis set. The solvent effects were further taken into account (*see infra*) through the Polarizable Continuum Model (PCM), using the integral equation formalism variant (IEFPCM).[30] These optimised structures allowed us to ascertain the dimensions of XB interactions (I···O distances and C-I···O angles) in gas-phase or in continuum solvent medium of water or acetonitrile. Their values are gathered in Table S6-1 and were used as reference in the subsequent determination of the I-EP (iodine-extra point) optimal distance for XB interactions between each substrate and **1.XB**.

Table S6-1. I···O distances (Å) in DFT optimisations of $\mathbf{1.XB_{ethyl}}$ model complexes

Optimisation conditions	Model Complex	
	$\mathbf{1.XB_{ethyl}}\cdot CH_3COO^-$	$\mathbf{1.XB_{ethyl}}\cdot H_2PO_4^-$
Gas-phase	2.473 ; 2.495	2.505 ; 2.505
Water model continuum	2.593 ; 2.629	2.665 ; 2.665
Acetonitrile model continuum	2.599 ; 2.635	2.672 ; 2.672

In our previous works on halide and sulfate recognition by macrocyclic halo-imidazolium receptors[31, 32] or rotaxane based halo-triazolium receptors,[33, 34] the XB interactions were described with resort to an extra point (EP) of charge added to GAFF.[35] Furthermore, this EP has van der Waals parameter and mass set to zero, a C-I-EP angle of 180° with a 150 kcal mol^{-1} rad^{-2} angle bending force constant and an I-EP optimal distance determined for each substrate model, with a 600 kcal mol^{-1} $Å^{-2}$ bond stretching force constant. This methodology was extended in this work to the enantioselective binding of chiral substrates mediated by XB bonds, as follows.

Different I-EP distances were systematically tested in gas-phase *via* MM energy minimisations of the model complexes between **1.XB** and CH_3COO^- or $H_2PO_4^-$ anions. To obtain atomic RESP charges adequate to XB interactions with the oxygen atoms of CH_3COO^- or $H_2PO_4^-$, the MM structure optimisations were preceded by the derivatisation of RESP charges at different I-EP distances. In a previously B3LYP/6-31G* optimised structure of **1.XB**, an extra point was positioned in front of each C-I bond at different I-EP distances and a C-I-EP angle of 180°. Subsequently, the electrostatic potential distribution of each structure, with two extra points at the same I-EP distances, was calculated followed by the RESP fitting (see below). Table S6-2 summarises the range of I-EP distances tested for two model complexes, as well as the I···O distances and the iodine and EP charges.

Table S6-2. Summary of gas-phase MM optimised I···O distances (Å) for **1.XB**·CH_3COO^- and **1.XB**·$H_2PO_4^-$, as function of the I-EP distance (Å), listed along with EP and iodine RESP charges.

I-EP distance	EP charge	I charge	**1.XB**·CH_3COO^-	**1.XB**·$H_2PO_4^-$
No EP	---	0.271700	5.701 ; 5.109	5.101 ; 3.306
1.95	0.111177	-0.033441	2.826 ; 2.823	2.859 ; 2.859
1.96	0.109979	-0.031382	2.812 ; 2.806	2.853 ; 2.852
1.97	0.108795	-0.029335	2.804 ; 2.798	2.845 ; 2.845
1.98	0.107623	-0.027300	2.803 ; 2.798	2.839 ; 2.838
1.99	0.106464	-0.025276	2.790 ; 2.785	2.831 ; 2.830
2.00	0.105317	-0.023263	2.782 ; 2.779	2.822 ; 2.822
2.01	0.104182	-0.021261	2.770 ; 2.772	2.814 ; 2.814
2.02	0.103060	-0.019270	2.757 ; 2.750	2.804 ; 2.803
2.03	0.101950	-0.017289	2.746 ; 2.738	2.792 ; 2.791
2.04	0.100850	-0.015317	Atomic clash	2.780 ; 2.779
2.05	0.099763	-0.013356	Atomic clash	2.765 ; 2.765
2.06	0.098685	-0.011403	Atomic clash	2.745 ; 2.745
2.07	0.097621	-0.009461	Atomic clash	2.714 ; 2.714
2.08	0.096566	-0.007527	Atomic clash	Atomic clash

Table S6-2 shows that several I-EP distances can be applied in the MM geometry optimisation of **1.XB**·CH_3COO^- and **1.XB**·$H_2PO_4^-$. On the other hand, the use of the longer I-EP distances (2.00 to 2.03 Å) in 300 K, 5 ns long, gas phase MD simulations of **1.XB**·CH_3COO^- was shown to be instable, being ruled out. For the gas phase MD simulations of **1.XB**·$H_2PO_4^-$, the same problem was verified for the I-EP distances between 2.02 and 2.07 Å. These MD simulations were extended to the other I-EP distances, and the 1.99 and 2.01 Å distances were found as best I-EP distances found carry out the MD simulations with complexes **1.XB**·CH_3COO^- and **1.XB**·$H_2PO_4^-$, respectively. Given that these two I-EP distances only differed by 0.02 Å, the shortest I-EP distance was selected for the subsequent MM calculations on the complexes of **1.XB** with CH_3COO^- or $H_2PO_4^-$. With the I-EP distance of 1.99 Å, equivalent I···O distances were obtained in solution (a solvent mixture composed of 1426 acetonitrile molecules and 42 water molecules, as described in Section S6.7), as shown in Table S6-3.

Table S6-3. Summary of solution MM optimised I···O distances (Å) for **1.XB**·CH_3COO^- and **1.XB**·$H_2PO_4^-$, for an I-EP distance of 1.99 Å.

Complex	**1.XB**·CH_3COO^-	**1.XB**·$H_2PO_4^-$
I···O distances (Å)	2.817 ; 2.852	2.857 ; 2.836

The I···O distances calculated for the structures of **1.XB**·CH_3COO^- and **1.XB**·$H_2PO_4^-$ optimised in solution by MM (Table S6-3) are only *ca.* 0.03 Å systematically longer than the distances obtained in the gas-phase MM optimisations (Table S6-2). On the other hand, the comparison presented in Table S6-1 between the I···O distances in model complexes of $\mathbf{1.XB_{ethyl}}$ shows that the inclusion of a solvent continuum of water or acetonitrile in DFT calculations leads to an increase of the I···O distances relatively to those computed in gas phase. Nevertheless, the I···O distances in both implicit solvent media compares fairly well with the I···O molecular mechanics distances in complexes of **1.XB**

obtained in the solvent mixture (Table S6-3). Hence, the I-EP distance of 1.99 Å was definitively selected for the further conformational analyses and MD simulations in the acetonitrile/water solvent mixture (Section S6-7).

S6.5 Calculation of RESP charges of receptors and substrates

The RESP charges of **1.XB** were derived in agreement with earlier parameterisation developed with **1.XB$_{ethyl}$** CH_3COO^- and $H_2PO_4^-$ complexes (previous section) considering one extra point of charge positioned in front of each iodine, at 1.99 Å distance and with a C-I-EP angle of 180°. This was preceded by initial optimisation of a single conformation of **1.XB** using B3LYP/6-31G*, followed by a single point calculation at the HF/6-31G* level, in agreement with the GAFF development (*vide supra*, Section S6.2). The final charges were then derived considering the position of the two extra points. Concerning **1.HB**, its RESP atomic charges were straightforwardly obtained at the HF/6-31G* level after an initial optimisation of a single conformation at the same level of theory.

The enantiomers *S* and *R* of each anionic substrate were optimised with the B3LYP functional along with the 6-31+G* basis set, followed by electrostatic potential calculation through a single point carried out at the HF/6-31G* theory level. The electrostatic potentials of both enantiomers were concatenated and the final atomic charges of either chiral substrate (*S* or *R*) were computed through a multi-conformation RESP fitting based on the individual atomic charges of two enantiomers.

S6.6 Triazolium ring force field parametrisation

The preliminary MM optimisations of **1.XB** or **1.HB**, with GAFF default parameters for the triazolium atom types (as assigned by *antechamber*[36] and depicted in red in Scheme S6-1) resulted in bond lengths and angles that poorly reproduced the bond lengths and angles observed in the triazolium moieties of the DFT optimised structures. Therefore, all distances within the triazolium ring, along with the C-I or C-H bond, and all angles affected by those bonds were reparametrised using structural data from quantum mechanics optimised structures. Five crystal structures, containing a 5-iodo-1,2,3-triazolium moiety were obtained from CCDC: Refcodes DAMNOW,[37] DAMNUC,[37] TACPEU,[38] TACPIY,[38] and TACPOE.[38] This series of molecules was extended with the addition of 5-iodo-1,3,4-trimethyl-*1H*-1,2,3-triazol-3-ium. All six structures were optimised at the B3LYP/6-31G* level. The bond lengths and angles obtained in the DFT optimised structures for the triazolium ring were averaged and used as equilibrium distances (r_{eq}) and equilibrium angles (θ_{eq}). Their values are listed in Table S6-4. The bond lengh and bond angles force constants (K_r and K_θ) were then calculated in agreement with the GAFT original paper.[19, 20]

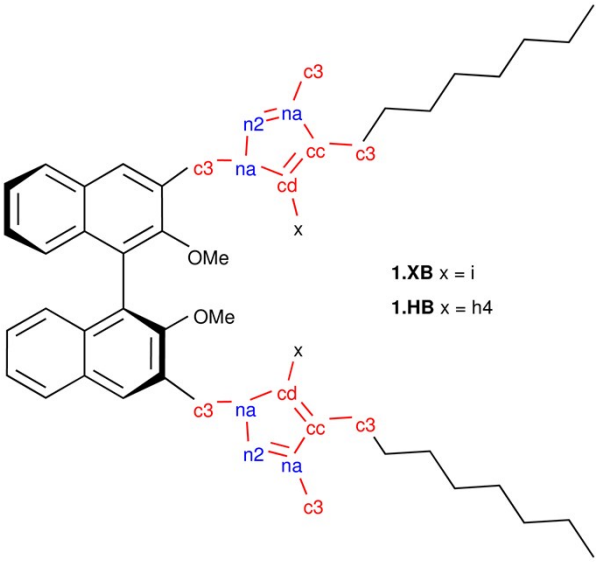

Scheme S6-1. GAFF atom types assigned for triazolium rings and carbon atoms attached of **1.XB** and **1.HB** by the *antechamber* utility.

Table S6-4. Force field parameters for the two triazolium moieties of **1.XB**.

Force field parameter	**GAFF default parameters**		**Quantum mechanics derived parameters**	
Bond lengths	r_{eq} (Å)	K_r (kcal mol^{-1} Å^{-2})	r_{eq} (Å)	K_r (kcal mol^{-1} Å^{-2})
na-n2	1.3685	503.9	1.3198	592.991
na-cc	1.3710	438.8	1.3691	441.535
na-cd	1.3710	438.8	1.3691	441.535
cc-cd	1.3710	504.0	1.3926	469.956
cd-i	2.1530	223.2	2.0838	258.576
Bond angles	θ_{eq} (°)	K_θ (kcal mol^{-1} rad^{-2})	θ_{eq} (°)	K_θ (kcal mol^{-1} rad^{-2})
na-n2-na	107.00	73.47	105.117	76.857
cc-cd-na	109.42	72.91	106.040	73.521
cd-cc-na	109.42	72.91	103.730	74.335
cc-na-n2	122.96	66.83	113.136	70.938
cd-na-n2	122.96	66.83	111.977	71.304
c3-na-n2	120.05	65.48	118.383	66.900
c3-na-cc	125.09	62.56	129.044	61.632
c3-na-cd	125.09	62.56	129.044	61.632
na-cd-i	121.61	59.37	124.900	58.781
cc-cd-i	123.70	57.46	129.038	56.438
cd-cc-c3[a)]	119.45	64.81	131.841	61.310
na-cc-c3[a)]	122.78	65.50	124.029	65.200

[a)] These angles were obtained directly from the DFT optimised structure of 5-iodo-1,3,4-trimethyl-*1H*-1,2,3-triazol-3-ium.

For the **1.HB** receptor, the same parameters were used for the triazolium motifs, apart the bond lengths and angles involving the prominent C-H binding units, which were assigned as cd-h4 and described with default GAFF parameters. Only the bending angles between Cd-H4 and triazolium adjacent atom types (cc-cd-h4) and (na-cd-h4) angles were changed, as summarised in Table S6-5.

Table S6-5. Additional force field parameters for the triazolium moiety of **1.HB**.

Force field parameter	**GAFF default parameters**		**Quantum mechanics derived parameters**	
Bond angles	θ_{eq} (°)	K_θ (kcal mol^{-1} rad^{-2})	θ_{eq} (°)	K_θ (kcal mol^{-1} rad^{-2})
na-cd-h4	119.66	50.22	124.900	49.212
cc-cd-h4	129.11	47.19	129.038	46.620

S6.7 General MD simulation methods

The starting binding geometry of each diastereoisomeric complex was obtained positioning the anion with the pertinent oxygen atoms of the carboxylate (*N*Boc-amino acid derivatives) or unbound oxygen atoms (BINOL-PO_4) in the vicinity of the binding units of **1.HB** or **1.XB**. Afterwards, all complexes underwent a MD run of 10 ns in gas-phase at 350 K and using a 1 fs time step length. 100000 structures were saved and further full energy minimised by means of MM until the convergence criterion of 0.0001 kcal mol^{-1} was achieved. In addition, the conformational analyses of the complexes of **1.HB** were undertaken with two 50 kcal mol^{-1} Å^{-2} C···O distance restraints, with C standing for each C-H binding unit carbon atom and O standing for the pertinent oxygen atom in the substrate) together with four 50 kcal mol^{-1} rad^{-2} angle restraints, two C-H···O and two H···O-A, where A stands for the carbon atom from carboxylate group in the *N*Boc-amino acid derivatives or for the phosphorus atom in BINOL-PO_4). This second series of restraints was applied to maintain the two C-H···O intermolecular interactions with an approximately linear binding geometry.

The lowest energy structure for each anion complex, was then solvated in a cubic box with 1426 acetonitrile molecules and 42 water molecules in agreement with a 99:1 v/v concentration used in ^{1}H NMR binding studies. One TBA and two PF_6^- counter-ions were added to neutralise the system net charge. Each solvated system was equilibrated under periodic boundary conditions using the following multistage protocol. The system was relaxed by MM minimisation of solvent molecules and by keeping the substrate, receptor and the counter-ion(s) fixed with a positional restraint of 500 kcal mol^{-1} Å^{-2}. The restraint was then removed and the entire system was allowed to relax. Both minimisation stages comprised an initial set of 10000 steepest descent algorithm steps, followed by 10000 steps of conjugated gradient algorithm. The equilibration stage proceeded with heating up the system to 300 K for 100 ps using a NVT ensemble and a weak positional restraint (10 kcal mol^{-1} Å^{-2}) on the solutes. Afterwards, each system was allowed to equilibrate in a NPT ensemble at 300 K and 1 atm for 1 ns. Finally, NPT data collection runs were carried out for 100 ns (for systems with **1.XB**) or for 50 ns (for systems with **1.HB**), with the trajectory frames being saved every 1 ps. Three independent replicates were performed for systems with **1.XB**, while five independent replicates were carried out for systems with **1.HB**. The CUDA version of the PMEMD executable was used for the simulation of all solvated systems.[39-41] The bond lengths involving all bonds to hydrogen atoms were constrained with the SHAKE algorithm allowing the usage of 2 fs time step.[42] The Particle Mesh Ewald (PME) method was used to treat the long-range electrostatic interactions.[43] The non-bonded van der Waals interactions were truncated with a 10 Å cut-off.

S6.8 Energetic assessment of MD simulations: $\Delta\Delta E_{bind(S,R)}$

All MD simulations were undertaken with equal number of molecules using the NPT ensemble. In these conditions, the binding energy (ΔE_{bind}) is equal to the enthalpy (ΔH_{bind}) and can be straightforwardly estimated from the MD runs as

$$\Delta E_{bind} = \langle E \rangle_{complex} + \langle E \rangle_{solvent} - \langle E \rangle_{\mathbf{1.XB}} - \langle E \rangle_{substrate}$$

where $\langle E \rangle_{complex,}$ $\langle E \rangle_{solvent}$, $\langle E \rangle_{\mathbf{1.XB}}$ and $\langle E \rangle_{substrate}$ are the average molecular mechanics (MM) energies of the complex, solvent, **1.XB** and chiral substrate, respectively.[44] The $\langle E \rangle_{solvent}$, $\langle E \rangle_{\mathbf{1.XB}}$ and $\langle E \rangle_{substrate}$ terms are accessed from individual MD simulations carried out in a NPT ensemble for the solvent mixture or with **1.XB** and chiral substrates solvated with same number of solvent molecules and adequately charge neutralised with counter-ions. On the other hand, the relative binding enthalpy associated with the enantioselective binding of **1.XB** towards a pair of *S*,*R* enantiomers of a substrate is just computed as

$$\Delta\Delta E_{bind(S,R)} = \langle E \rangle_{complex,S} - \langle E \rangle_{complex,R}$$

giving that the $\langle E \rangle_{solvent}$, $\langle E \rangle_{\mathbf{1.XB}}$ and $\langle E \rangle_{substrate}$ terms are cancelled. $\Delta\Delta E_{bind(S,R)}$ energy accounts the differences on the strength of the interaction of **1.XB** with *S* and *R* enantiomers, as well as eventual different interactions between the solvent molecules and the two diastereoisomeric complexes.

S6.9 DFT methods

The starting geometries of each diastereoisomeric complex of **1.XB** for geometry optimisations were the most frequent structures obtained from the cluster analysis of the 300 ns of MD trajectories, after striping the solvent molecules and counter-ions. As the complexes of **1.HB** were not stable throughout the MD simulations, the starting geometries of the diastereoisomers complexes of **1.HB** were generated from the **1.XB** corresponding ones by replacement of the iodine triazolium substituents by hydrogen atoms. All complexes were optimised with the M06-2X functional along with the 6-31G* basis set.

The distribution of electrostatic potential, $V(r)$, on the molecular surfaces of **1.XB** and **1.HB** was computed at the M06-2X/6-31G* level from previously optimised structures of their complexes with *N*Boc-(*S*)-tryptophan substrate, after removal of chiral substrate of the corresponding complex. In this work, the $V(r)$ was evaluated on the 0.001 electrons Bohr^{-3} contour of $\rho(r)$, and is henceforth labelled $V_S(r)$. The electrostatic potential surface ranges, between the most negative and most positive values ($V_{S,min}$ and $V_{S,max}$, respectively), was ascertained using the *multiwfn* program.[45, 46]

The Wiberg bond indices (WBI)[47] which consist in the sum of squares of off-diagonal density matrix elements between atoms. In this study, the WBI were ascertained from the DFT optimized structures of the diastereoisomeric complexes of **1.XB** or **1.HB**. These calculations were carried out using the Natural Bond Orbital (NBO) Version 3.1 program,[48, 49] within the Gaussian09 suite, at the M06-2X/6-

31G* level. The values given in Table S5-3 are the sum of all WBI concerning the iodine (**1.XB**) or hydrogen atoms (**1.HB**) of each receptor binding units and the pertinent oxygen atoms in the substrates.

S7. References

1. B. Y. Lee, S. R. Park, H. B. Jeon and K. S. Kim, *Tetrahedron Lett.*, 2006, **47**, 5105-5109.
2. J. K. Ou-Yang, Y. Y. Zhang, M. L. He, J. T. Li, X. Li, X. L. Zhao, C. H. Wang, Y. Yu, D. X. Wang, L. Xu and H. B. Yang, *Org. Lett.*, 2014, **16**, 664-667.
3. W. S. Brotherton, R. J. Clark and L. Zhu, *J. Org. Chem.*, 2012, **77**, 6443-6455.
4. A. Kormos, I. Moczar, D. Pal, P. Baranyai, J. Kupai, K. Toth and P. Huszthy, *Tetrahedron-Asymmetr*, 2013, **24**, 62-65.
5. M. J. Hynes, *J Chem Soc Dalton*, 1993, DOI: DOI 10.1039/dt9930000311, 311-312.
6. Kratochv.B, E. Lorah and C. Garber, *Anal. Chem.*, 1969, **41**, 1793-&.
7. S. M. MacDonald and S. G. Roscoe, *Electrochim. Acta*, 1997, **42**, 1189-1200.
8. F. H. Allen, *Acta crystallographica. Section B, Structural science*, 2002, **58**, 380-388.
9. Y. C. Qin, L. Liu, M. Sabat and L. Pu, *Tetrahedron*, 2006, **62**, 9335-9348.
10. L. Van Meervelt, K. De Wael and T. Zeegers-Huyskens, *J. Mol. Struct.*, 1995, **356**, 183-190.
11. P. Sahoo, R. Sankolli, H. Y. Lee, S. R. Raghavan and P. Dastidar, *Chem. Eur. J.*, 2012, **18**, 8057-8063.
12. G. Blaser, J. M. Sanderson, A. S. Batsanov and J. A. K. Howard, *Tetrahedron Lett.*, 2008, **49**, 2795-2798.
13. L. Fadini and A. Togni, *Tetrahedron-Asymmetr*, 2008, **19**, 2555-2562.
14. R. Taylor and C. F. Macrae, *Acta crystallographica. Section B, Structural science*, 2001, **57**, 815-827.
15. I. J. Bruno, J. C. Cole, P. R. Edgington, M. Kessler, C. F. Macrae, P. McCabe, J. Pearson and R. Taylor, *Acta crystallographica. Section B, Structural science*, 2002, **58**, 389-397.
16. C. F. Macrae, P. R. Edgington, P. McCabe, E. Pidcock, G. P. Shields, R. Taylor, M. Towler and J. van De Streek, *J. Appl. Crystallogr.*, 2006, **39**, 453-457.
17. C. F. Macrae, I. J. Bruno, J. A. Chisholm, P. R. Edgington, P. McCabe, E. Pidcock, L. Rodriguez-Monge, R. Taylor, J. van de Streek and P. A. Wood, *J. Appl. Crystallogr.*, 2008, **41**, 466-470.
18. Gaussian 09, Revision A.01, M. J. Frisch, G. W. Trucks, H. B. Schlegel, G. E. Scuseria, M. A. Robb, J. R. Cheeseman, G. Scalmani, V. Barone, B. Mennucci, G. A. Petersson, H. Nakatsuji, M. Caricato, X. Li, H. P. Hratchian, A. F. Izmaylov, J. Bloino, G. Zheng, J. L. Sonnenberg, M. Hada, M. Ehara, K. Toyota, R. Fukuda, J. Hasegawa, M. Ishida, T. Nakajima, Y. Honda, O. Kitao, H. Nakai, T. Vreven, J. A. Montgomery, Jr., J. E. Peralta, F. Ogliaro, M. Bearpark, J. J. Heyd, E. Brothers, K. N. Kudin, V. N. Staroverov, R. Kobayashi, J. Normand, K. Raghavachari, A. Rendell, J. C. Burant, S. S. Iyengar, J. Tomasi, M. Cossi, N. Rega, J. M. Millam, M. Klene, J. E. Knox, J. B. Cross, V. Bakken, C. Adamo, J. Jaramillo, R. Gomperts, R. E. Stratmann, O. Yazyev, A. J. Austin, R. Cammi, C. Pomelli, J. W. Ochterski, R. L. Martin, K. Morokuma, V. G. Zakrzewski, G. A. Voth, P. Salvador, J. J. Dannenberg, S. Dapprich, A. D. Daniels, Ö. Farkas, J. B. Foresman, J. V. Ortiz, J. Cioslowski, and D. J. Fox, Gaussian, Inc., Wallingford CT, 2009.
19. J. Wang, R. M. Wolf, J. W. Caldwell, P. A. Kollman and D. A. Case, *J. Comput. Chem.*, 2004, **25**, 1157-1174.
20. J. Wang, R. M. Wolf, J. W. Caldwell, P. A. Kollman and D. A. Case, *J. Comput. Chem.*, 2005, **26**, 114-114.
21. K. A. Peterson, D. Figgen, E. Goll, H. Stoll and M. Dolg, *J. Chem. Phys.*, 2003, **119**, 11113-11123.
22. K. A. Peterson, B. C. Shepler, D. Figgen and H. Stoll, *J. Phys. Chem. A*, 2006, **110**, 13877-13883.
23. D. Feller, *J. Comput. Chem.*, 1996, **17**, 1571-1586.
24. K. L. Schuchardt, B. T. Didier, T. Elsethagen, L. Sun, V. Gurumoorthi, J. Chase, J. Li and T. L. Windus, *J. Chem. Inf. Model.*, 2007, **47**, 1045-1052.
25. D.A. Case, J.T. Berryman, R.M. Betz, D.S. Cerutti, T.E. Cheatham, III, T.A. Darden, R.E. Duke, T.J. Giese, H. Gohlke, A.W. Goetz, N. Homeyer, S. Izadi, P. Janowski, J. Kaus, A. Kovalenko, T.S. Lee, S. LeGrand, P. Li, T. Luchko, R. Luo, B. Madej, K.M. Merz, G. Monard, P. Needham, H. Nguyen, H.T. Nguyen, I. Omelyan, A. Onufriev, D.R. Roe, A. Roitberg, R. Salomon-Ferrer, C.L. Simmerling, W. Smith, J. Swails, R.C. Walker, J. Wang, R.M. Wolf, X. Wu, D.M. York and P.A. Kollman (2015), AMBER 2015, University of California, San Francisco.
26. C. I. Bayly, P. Cieplak, W. D. Cornell and P. A. Kollman, *J. Phys. Chem.*, 1993, **97**, 10269-10280.
27. Z. Liu, S. Huang and W. Wang, *The Journal of Physical Chemistry B*, 2004, **108**, 12978-12989.

28. X. Grabuleda, C. Jaime and P. A. Kollman, *J. Comput. Chem.*, 2000, **21**, 901-908.
29. D. R. Roe and T. E. Cheatham, *J. Chem. Theory Comput.*, 2013, **9**, 3084-3095.
30. S. Miertuš, E. Scrocco and J. Tomasi, *Chem. Phys.*, 1981, **55**, 117-129.
31. A. Caballero, F. Zapata, N. G. White, P. J. Costa, V. Felix and P. D. Beer, *Angew. Chem. Int. Ed. Engl.*, 2012, **51**, 1876-1880.
32. F. Zapata, A. Caballero, N. G. White, T. D. Claridge, P. J. Costa, V. Felix and P. D. Beer, *J. Am. Chem. Soc.*, 2012, **134**, 11533-11541.
33. M. J. Langton, S. W. Robinson, I. Marques, V. Felix and P. D. Beer, *Nat Chem*, 2014, **6**, 1039-1043.
34. M. J. Langton, I. Marques, S. W. Robinson, V. Felix and P. D. Beer, *Chem. Eur. J.*, 2016, **22**, 185-192.
35. M. A. Ibrahim, *J. Comput. Chem.*, 2011, **32**, 2564-2574.
36. J. Wang, W. Wang, P. A. Kollman and D. A. Case, *J. Mol. Graph. Model.*, 2006, **25**, 247-260.
37. N. L. Kilah, M. D. Wise and P. D. Beer, *Crystal Growth & Design*, 2011, **11**, 4565-4571.
38. N. L. Kilah, M. D. Wise, C. J. Serpell, A. L. Thompson, N. G. White, K. E. Christensen and P. D. Beer, *J. Am. Chem. Soc.*, 2010, **132**, 11893-11895.
39. R. Salomon-Ferrer, A. W. Gotz, D. Poole, S. Le Grand and R. C. Walker, *J. Chem. Theory Comput.*, 2013, **9**, 3878-3888.
40. A. W. Gotz, M. J. Williamson, D. Xu, D. Poole, S. Le Grand and R. C. Walker, *J. Chem. Theory Comput.*, 2012, **8**, 1542-1555.
41. S. Le Grand, A. W. Götz and R. C. Walker, *Comput. Phys. Commun.*, 2013, **184**, 374-380.
42. J.-P. Ryckaert, G. Ciccotti and H. J. C. Berendsen, *J. Comput. Phys.*, 1977, **23**, 327-341.
43. T. Darden, D. York and L. Pedersen, *J. Chem. Phys.*, 1993, **98**, 10089.
44. A. T. Fenley, N. M. Henriksen, H. S. Muddana and M. K. Gilson, *J. Chem. Theory Comput.*, 2014, **10**, 4069-4078.
45. T. Lu and F. Chen, *J. Mol. Graph. Model.*, 2012, **38**, 314-323.
46. T. Lu and F. Chen, *J. Comput. Chem.*, 2012, **33**, 580-592.
47. K. B. Wiberg, *Tetrahedron*, 1968, **24**, 1083-1096.
48. E. D. Glendening, A. E. Reed, J. E. Carpenter and F. Weinhold., *Journal*.
49. A. E. Reed, L. A. Curtiss and F. Weinhold, *Chem. Rev.*, 1988, **88**, 899-926.